

Topology of plane sections of periodic polyhedra with an application to the Truncated Octahedron

Roberto De Leo*

November 19, 2018

Abstract

The main results of A. Zorich and I. Dynnikov about plane sections of periodic surfaces are extended to the PL case. As an application, the Stereographic Map of a truncated octahedron, extended to the whole \mathbb{R}^3 by periodicity, is analyzed numerically.

1 Introduction

The problem of the asymptotics of plane sections of smooth periodic surfaces, extracted from Physics literature by S.P. Novikov in 1982 [Nov82], turned out to be much richer than expected, leading ultimately to the association of a fractal on \mathbb{RP}^2 to every element of a large class of triply periodic functions in \mathbb{R}^3 (see Section 2).

In order to visualize for the first time Stereographic Maps associated to triply periodic smooth functions and to get numerical confirmations of a Novikov conjecture, claiming that the Hausdorff dimension of such fractals is strictly between 1 and 2, we developed a C++ library and used it to investigate two smooth cases [Leo03]. Unfortunately, the running time of our numerical explorations grows way too much as soon as we sample with resolutions big enough to get a hint of the fractals, mainly because the number of polygons of the meshes approximating curved smooth surfaces (e.g. to retrieve its intersection with a plane) gets soon very big.

This fact suggests that, from the numerical point of view, polyhedra are the best surfaces to study, at the very least for the obvious reason that the number of polygons needed to describe them at any resolution is constant. Moreover, such constant can be rather small even in non trivial cases, e.g. like in the case of the “extended truncated octahedron”, presented in this paper, which has just eight hexagonal faces.

*INFN <roberto.deleo@ca.infn.it>, Dept. Physics, U. of Cagliari and Dept. of Mathematics, U. of Cagliari <deleo@unica.it>, Cagliari, Italy.

Since the main results of the theory, due to A.V. Zorich [Zor84] and I.A. Dynnikov [Dyn97, Dyn99], refer to the case of smooth surfaces only, in Section 2 we will provide independent proofs for those theorems that make use of the smooth structure and will mention the main properties of the system. Then, in Section 3, we present the algorithm we implemented to explore numerically the problem and the results obtained in case of a the polyhedron obtained extending by periodicity the truncated octahedron.

2 Fundamental objects and theorems

2.1 Critical Points of height functions in polyhedra

An analog of the Morse theory for height functions on polyhedra has been introduced by T. Banchoff in [Ban67, Ban70]. Here we recall the concepts relevant for the present paper, slightly modified to cover the case of periodic polyhedra.

Definition 1. By “*embedded polyhedron*” $M \subset \mathbb{R}^3$ we mean a countable collection of cells $K = \{C^r \subset \mathbb{R}^3\}_{r=0,1,2}$, where 0-cells are points (vertices), 1-cells are closed connected segments and 2-cells are convex closed plane polygons, such that:

- P1* the boundary of any cell is union of cells of lesser degree;
- P2* every cell having points in common with a higher degree cell is completely contained inside it;
- P3* K is locally finite, i.e. every vertex has a neighborhood in \mathbb{R}^3 that intersects only finitely many cells;
- P4* for any point $p \in M$, the union $\text{Star}(p)$ of all cells containing that point is omeomorphic to an open disc.

A triply periodic polyhedron is a polyhedron that is invariant with respect to a rank-3 discrete subgroup $\Gamma \simeq \mathbb{Z}^3$ of \mathbb{R}^3 . Finally, by polyhedron $\mathcal{M} \subset \mathbb{T}^3$ we mean the quotient $M/\Gamma \subset \mathbb{R}^3/\Gamma \simeq \mathbb{T}^3$ of a triply periodic polyhedron.

Every triply periodic polyhedron M embedded in \mathbb{R}^3 is the lift of a compact polyhedron \mathcal{M} embedded in \mathbb{T}^3 . Since we are going to study polyhedra’s plane foliations, we are interested in the reciprocal relation between polyhedra and height functions (or, equivalently, constant 1-forms):

Definition 2. A height function $h(p) = h^\alpha p_\alpha$ is called “*generic*” for the polyhedron M if no edge of M is perpendicular to the direction $\mathbf{H} = (h^\alpha)$. Equivalently, a constant 1-form $\omega = h^\alpha dp_\alpha$ in \mathbb{R}^3 (resp. \mathbb{T}^3) is generic for M (resp. \mathcal{M}) if no edge of M (resp. \mathcal{M}) is contained in a single leaf¹ of ω .

¹Frobenius theorem grants that the distribution $\omega = 0$ is integrable iff the 1-form ω is closed. In this case, the leaves induced by $\omega = h^\alpha dp_\alpha$ in \mathbb{T}^3 are the projections of the \mathbb{R}^3 planes perpendicular to $\mathbf{H} = (h^\alpha)$; those induced on a polyhedron \mathcal{M} are the intersections of these leaves with the polyhedron.

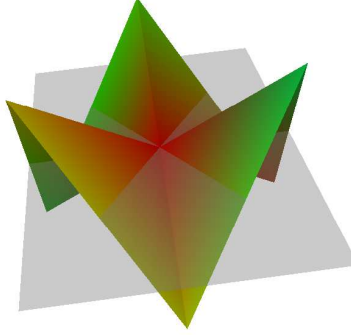


Figure 1: Piece-wise linear Monkey Saddle: in the smooth case, a however small perturbation would be enough to resolve this critical point in a pair of elementary saddles; in the piece-wise linear case instead it is stable and, therefore, generic.

Since height functions are not single-valued on \mathbb{T}^3 (unless \mathbf{H} is an integer direction, i.e. parallel to a lattice vector) while their differentials $\omega = dh$ are always well-defined in both \mathbb{R}^3 and \mathbb{T}^3 , we will refer mostly to 1-forms from now on. From the definition above it is clear that, like in the smooth case, the set of non-generic 1-forms has zero measure.

Note that the foliation induced on \mathbb{T}^3 (and therefore on \mathcal{M}) by ω does not change by multiplying the 1-form by a non-zero scalar, so from now on we will think of ω at the same time as a constant 1-form and as a point in \mathbb{RP}^2 .

Definition 3. *The index of a point $p \in M$ (or, equivalently, $[p] \in \mathcal{M}$) with respect to a generic constant 1-form ω is the integer $i(p, \omega) = 1 - s/2$, where s is the number of segments, having p as one of their extremes, in which the leaf of ω passing through p cuts $\text{Star}(p)$. If $i(p, \omega) = 0$, i.e. if the $\text{Star}(p)$ is cut in exactly two components, the point is said “regular”; otherwise it is called “critical”.*

The set of critical points for any generic constant 1-form is of course a subset of the set of vertices; exactly as in the smooth case, minima and maxima have index $+1$ and non-degenerate saddles have index -1 . The main difference between the smooth and the piece-wise linear (PL) case, for our purposes, is that saddles that are unstable in the former case, i.e. disappear for small perturbations of the 1-form direction, are stable in the latter and therefore cannot be disregarded; the simplest example is provided by the “Monkey saddle”, which has index -2 (see Figure 1).

Nevertheless, an analog of the critical point theorem for generic 1-forms holds:

Theorem 1. *If M is a triply periodic polyhedron, invariant by the action of the rank-3 group $\Gamma \subset \mathbb{Z}^3$, and ω is generic for M , then $\sum_{[p] \in \mathcal{M}} i(p, \omega) = \chi(\mathcal{M})$,*

where $[p]$ is the set of vertices Γ -equivalent to p and the sum is hence extended to any set of inequivalent vertices. Equivalently, if we set to 1 the volume of a Dirichlet domain of Γ , then the average of the Euler characteristic of M converges to the Euler characteristic of \mathcal{M} :

$$\overline{\chi(M)} = \lim_{R \rightarrow \infty} \sum_{\|p\| < R} i(p, \omega) / \text{Vol}(B_R) = \chi(\mathcal{M})$$

Proof. Since Banchoff's proof [Ban70] of the critical point theorem for polyhedra is only based on local identities that are trivially true also in \mathbb{T}^3 , that proof holds with no change for our case.

The second part can be proved by considering that the genus g of the surface \mathcal{M} contained inside a cube of side R can be evaluated by reducing by homotopy the surface to a graph and then evaluating the rank of the graph's first homology group. The result follows from the consideration that every component contained in a inner unitary cube contributes by g to the total genus of the component contained in the cube of radius R and their number grows with R^3 , while the cubes on the boundary provide a smaller contribute but can be disregarded in the limit for $R \rightarrow \infty$ since their number grows only as R^2 . \square

2.2 Structure of foliations

In the most general case, a constant 1-form ω induces on a triply periodic polyhedron M both open and closed leaves.

Since being homotopic to zero is an open condition, leaves close enough to closed ones are also closed; maximal components of closed leaves are always enclosed between a pair of critical points of ω on M and form either cylinders (when both critical points are saddles) or discs (when one is a saddle and the other is a center) or spheres (when they are both centers). The last two cases are topologically trivial: a disc covered by closed leaves around a center is exactly a homotopy to a point of that component of M , and if M is a sphere then no open orbit can ever be induced on it by a closed 1-form. Hence, once the topologically trivial components are removed, what is left is a collection of cylinders \mathcal{C}_i that separates a collection of subpolyhedra with boundary \mathcal{N}_i filled by open leaves.

Definition 4. A genus- k component of \mathcal{M} is a PL submanifold with boundary \mathcal{N} of \mathcal{M} such that:

1. $\partial\mathcal{N}$ is the finite disjoint union of plane parallel (topological) circles homotopic to zero;
2. the closed polyhedron $\overline{\mathcal{N}}$, obtained by filling \mathcal{N} 's holes with plane discs, has genus k .

Definition 5. A Dynnikov decomposition \mathcal{Z} of a polyhedron \mathcal{M} is a collection of subpolyhedra with boundary $\{\mathcal{C}_i, \mathcal{N}_j\}$ of \mathcal{M} such that:

1. every \mathcal{C}_i is homotopic either to a closed cylinder or to a closed disc;

2. every \mathcal{N}_j is a genus- k_j component of \mathcal{M} ;
3. $i \neq j \implies \mathcal{N}_i \cap \mathcal{N}_j = \emptyset$, while every other pair of distinct subpolyhedra of \mathcal{Z} that is not disjoint shares single a boundary component;
4. $\mathcal{M} = \bigcup_i \mathcal{C}_i \bigcup_j \mathcal{N}_j$.

The genus and rank of a Dynnikov decomposition \mathcal{Z} are, respectively, the highest genus and rank of the $\overline{\mathcal{N}}_j$ s contained in \mathcal{Z} ; a genus-1 rank-2 Dynnikov decomposition is called “Zorich decomposition”.

From the considerations above it is clear that every constant 1-form ω in general position with respect to \mathcal{M} , i.e. such that there are no saddle connections, induces naturally a Dynnikov decomposition \mathcal{Z} on \mathcal{M} where all \mathcal{C}_i are filled by the closed leaves and all \mathcal{N}_j by the open ones.

Under the same assumptions, to every focus it is associated a saddle that “cancels” it, namely there’s a homotopy of the surface that gets rid of the pair saddle-focus without modifying the topology of the open orbits nearby; we call the saddle-type critical points that are left “topological saddles”, since it is them that contribute to the Euler characteristic of the surface.

In the smooth generic case, the number of Γ -inequivalent topological saddles, i.e. the number of topological saddles in \mathcal{M} , is of course exactly equal to $2g-2$; in the PL case however, since we can have generic saddles with higher multiplicity, the Euler characteristic is only an upper bound for the number of topological saddles, as $\chi(\mathcal{M}) = 2 - 2g = \sum_{k \in \mathbb{Z}} k \cdot \#\{[p] | i(\omega, p) = k\}$.

2.3 The close-to-rational case

Definition 6. By “irrationality degree” of a closed 1-form Ω on a piecewise smooth manifold M we mean the number of rationally independent integrals of Ω over any base of the homology integer 1-cycles of M : $\text{irr}(\Omega) = \dim_{\mathbb{Q}} \text{span}_{\mathbb{Q}} \{\int_{\gamma} \Omega\}$, $\gamma \in H_1(M, \mathbb{Z})$; 1-irrational forms are also called “rational”.

The structure of foliations induced on a periodic polyhedron by rational 1-forms is much simpler than in the generic case since in this case all leaves are periodic; moreover, the appearance of a topological invariant enforces all 1-forms close enough to rational to show the same behaviour.

Rational 1-forms are rather special because foliations induced on \mathcal{M} by them are also induced by well-defined circle-valued functions on the polyhedron: indeed, if $\{\gamma_i\}_{i=1,2,3}$ is a base for $H_1(\mathbb{T}^3, \mathbb{R})$ and N an integer big enough such that $N \int_{\gamma_i} \omega \in \mathbb{Z}$, $i = 1, 2, 3$, and $p_0 \in \mathcal{M}$, then the function

$$f : M \longrightarrow \mathbb{S}^1$$

$$p \mapsto \exp(iN \int_{p_0}^p \omega)$$

is well defined and differentiable, and its differential $df_p = iN\omega_p f(p)$ is proportional to ω ; since f is never zero, the set $df = 0$ on M coincides with the restriction to M of $\omega = 0$.

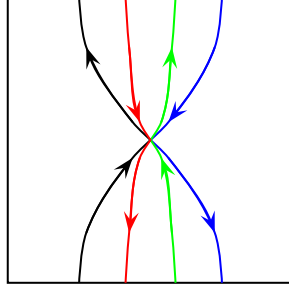


Figure 2: A (hypothetical) saddle point where four open leaves meet simultaneously: the two branches of each of the inner open leaves cannot be adjacent to each other, so this picture cannot come from the section of a locally euclidean surface.

This shows that all leaves induced by rational 1-forms on a polyhedron $\mathcal{M} \subset \mathbb{T}^3$ are compact and therefore corresponding leaves on $M \subset \mathbb{R}^3$ will be open or closed according to their homology class: leaves homotopic to zero in \mathbb{T}^3 will remain so in any covering, all others will open up in \mathbb{T}^3 's universal covering.

Definition 7. From now on we will refer to closed leaves non homotopic to zero as “periodic” or, more generically, “open” leaves, so that by “closed leaf” we will implicitly mean a closed leaf homotopic to zero.

Lemma 1. Be ω a rational 1-form in general position with respect to a polyhedron \mathcal{M} : then no more than two open leaves can collide at any saddle point.

Proof. The 1-form ω foliates \mathbb{T}^3 in a 1-parameter family of embedded 2-tori, so that all open leaves at the same level of ω are parallel (i.e. they represent the same 1-cycle modulo sign); moreover the number of open leaves on every level is even, since they are all indivisible and their sum must be zero.

It is easy to check, just by drawing pictures, that it is possible to have saddles of any index with closed leaves, and adding a single pair of open leaves does not change this situation; their presence though does not allow the presence of any other pair, since in any saddle point the two extremes of the same (critical) leaf must appear next to each other and this is of course impossible for all open leaves, apart for the two most external ones (e.g. see Figure 2). \square

Theorem 2. The Dynnikov decomposition induced on \mathcal{M} by any constant rational 1-form in general position is Zorich.

Proof. Since all (non critical) leaves induced by ω on \mathcal{M} are circles, the critical points of ω on \mathcal{M} determine a subdivision of the polyhedron in the connected sum of a finite number of cobordisms. In the smooth case, the only non trivial cobordisms are elementary (i.e. pants-like) and Zorich [Zor84] proved that in

the boundary of each part there is at least one of the three boundary loops that is homotopic to zero (in \mathbb{T}^3), from which the theorem follows easily.

In the polyhedra case the cobordisms are not necessarily elementary, i.e. more than two leaves may collide at a saddle point, but lemma 1 grants us that even in this case no more than two loops in the cobordism may be open. This shows that the components of open leaves have genus 1 and therefore the decomposition induced on \mathcal{M} by ω is Zorich. \square

The presence of a genus-1 rank-2 component of open leaves is a very strong condition and leads to the appearance of a topological quantity associated to the foliation [Dyn97]:

Theorem 3. *A Dynnikov decomposition \mathcal{Z} of \mathcal{M} with rank 2 has genus 1 if and only if at least one of its \mathcal{N}_j embedded with rank 2 has genus 1. In this case, all \mathcal{N}_j are genus-1 components of \mathcal{M} and those embedded with rank 2 represent, modulo sign, the same indivisible non-zero 2-homology class in \mathbb{T}^3 .*

Definition 8. *We call “soul” of a Zorich decomposition \mathcal{Z} the “unsigned” non-trivial indivisible homology class $l \in PH_2(\mathbb{T}^3, \mathbb{Z})$ common to all rank-2 components of \mathcal{Z} .*

Corollary 1. *Be ω a rational 1-form inducing on \mathcal{M} a rank-2 Zorich decomposition \mathcal{Z} : then any 1-form ω' close enough to ω induces on \mathcal{M} a rank-2 Zorich decomposition \mathcal{Z}' and this decomposition is homotopic to \mathcal{Z} . In particular, all such decompositions share the same soul, i.e. the soul is a locally constant function of the pair (\mathcal{M}, ω) .*

Proof. The leaves at the boundary between \mathcal{M} 's genus-1 components of periodic leaves \mathcal{N}_i and the cylinders of closed leaves are themselves closed and therefore stable under small perturbations of ω 's direction; consequently, no cylinder of closed orbits will disappear in a whole neighborhood of $\omega \in \mathbb{RP}^2$. Since no two leaves of a foliation can intersect, this means that open leaves are bounded to genus-1 components of \mathcal{M} , homotopic to the \mathcal{Z} ones, even for all 1-forms close enough to ω .

Finally, since the homology class l of these rank-2 genus-1 components is integer and they change continuously, this l must be the same (modulo sign) for all them. \square

The soul l of a Zorich decomposition is a fundamental invariant since its knowledge is enough to describe the asymptotic behaviour of the open leaves. Indeed, the fact that $[\mathcal{N}_i] = \pm l$ means that, in \mathbb{R}^3 , the lift $\hat{\mathcal{N}}_i$ of \mathcal{N}_i lies between a pair of parallel planes perpendicular to l (seen as a direction in \mathbb{R}^3), so that the lift to \mathbb{R}^3 of an open leaf, namely an open intersection of $\hat{\mathcal{N}}_i$ with a plane perpendicular to ω (seen as a vector in \mathbb{R}^3), is a curve contained in a plane strip of finite width; Dynnikov [Dyn92] showed how these conditions are enough to conclude that the leaf is actually a finite deformation of a straight line whose direction is the axis of the strip, namely “ $\omega \times l$ ”.

Since the foliation induced by ω is determined just by its direction \mathbf{H} and the soul itself can be interpreted as a direction in \mathbb{R}^3 , once we fix a surface M we can think the soul application as a locally constant application $\text{soul}_{\mathcal{M}} : \mathbb{RP}^2 \rightarrow \mathbb{RP}^2$. We will show in next section that, for a generic polyhedron \mathcal{M} , this map is well defined on the whole projective plane except for a set of measure zero (“ergodic directions”) and its image amounts to a finite number of points.

Definition 9. *The non-empty level sets $\mathcal{D}_l(\mathcal{M}) = \text{soul}_{\mathcal{M}}^{-1}(l)$ corresponding to non-zero values of l are called “islands” or “stability zones” of \mathcal{M} . The union of all stability zones $\mathcal{S}(\mathcal{M}) = \cup_l \mathcal{D}_l(\mathcal{M})$ is called the “Stereographic Map” (SM) of \mathcal{M} .*

Strange as it seems, this whole construction is the natural model for a very concrete physical phenomenon, namely the magnetoresistance in normal metals, with the periodic surface being the “Fermi Surface” of a metal, the 1-form a strong constant homogenous external magnetic field and the Fermi Surface leaves the orbits of the momenta of the metal’s quasi-electrons. The presence of open leaves is detectable experimentally, and so is each stability zone (provided at least two points of it are measured [NM98]). Experimental plots of the SM have been produced in Sixties and Seventies for about thirty metals but only recently the first two SM, relative to the Fermi Surfaces of Au and Ag, have been reproduced theoretically from first first principles [Leo04b, Leo05b].

2.4 The generic (3-irrational) case

In the previous section we showed that the structure of the foliation in a neighborhood of rational directions is rather simple: either all leaves are closed or their lift is strongly asymptotic to a straight line [Dyn97], i.e. it is contained in a finite-width plane strip and crosses it from one end to the other. Still, this is far from being enough, since the sole density of an open set does not preclude its measure from being small.

We will prove in this section that the one above is nevertheless the generic situation, namely:

Theorem 4. *The set of directions in \mathbb{RP}^2 inducing Dynnikov decompositions of genus bigger than one on a generic polyhedron \mathcal{M} has measure zero.*

To prove this theorem, Dynnikov studied the structure of the foliation induced by a 3-irrational 1-form ω on 1-parameter family of surfaces $M_e = f^{-1}(e)$, where f is a triply periodic Morse function such that for almost all values of f no more than one critical point of ω lies on the same leaf. Here, we will repeat Dynnikov’s steps assuming f to be a generic triply periodic PL function, so that almost all of its level surfaces are embedded polyhedra, satisfying the same genericity condition with respect to ω .

The following two lemmas by Dynnikov extend with no change to the polyhedra case:

Lemma 2. *Given a triply periodic PL function, the set of values for which a constant 1-form ω induces open leaves filling rank-2 components is a closed connected interval $[e_1(\omega), e_2(\omega)]$. The functions e and E are continuous on the whole \mathbb{RP}^2 .*

Definition 10. *The Dynnikov index w of a critical point c of $\omega = h^\alpha dp_\alpha$ with respect to an oriented polyhedron \mathcal{M} is the product of the “Hamiltonian” index of the critical point (+1 for centers and -1 for saddles) times the sign of the scalar product between $\mathbf{H} = (h^\alpha)$ and any of the normals to the faces adjacent to the critical vertex.*

Lemma 3. *The curve $\gamma_{\omega,f}(e) = \sum_i w_i c_i(e)$ is a well defined loop in \mathbb{T}^3 and the quantity*

$$\bar{\chi}_{\omega,f}(e) = \int_{-\infty}^e i_{\gamma_{\omega,f}}^* \omega$$

is equal to the density of closed leaves on any leaf induced by ω on \mathbb{T}^3 .

Moreover, if $\{h_j^+\}$ (resp. $\{h_k^-\}$) are the heights of the “positive” (resp. “negative”) cylinders of closed leaves on \mathcal{M} , namely those that contain points with smaller (resp. bigger) values of f , it turns out that it is possible to choose \mathbb{R}^3 representative \hat{c}_i of the critical points so that

$$\bar{\chi}_{\omega,f}(e) = \sum_i \langle \mathbf{H}, w_i \hat{c}_i(e) \rangle = \sum_j h_j^+ - \sum_k h_k^-$$

In the weighted sum of all critical points are also contained the pairs center-saddle, that can be removed by homotopy and have nothing to do with the topology of the foliation. If we do not include them in the summation, we are left with a new quantity that tells us the density of non-trivial (in \mathcal{M}) closed leaves and therefore is able to spot whether there are cylinders of non-zero heights. In particular, to have a full ergodic situation, i.e. a leaf dense on the whole \mathcal{M} , this function must necessarily be zero.

Lemma 4. *Be $\{c_i^{top}\}$ the subset of the topological saddles of the pair (ω, f) . Then the reduced curve $\gamma_{\omega,f}^{top}(e) = \sum_i w_i c_i^{top}(e)$ is also well-defined in \mathbb{T}^3 and the reduced Euler density $\bar{\chi}_{\omega,f}^{top}(e) = \int_{-\infty}^e i_{\gamma_{\omega,f}^{top}}^* \omega$ is equal to the density of closed leaves non homotopic to zero in \mathcal{M} .*

The function $\bar{\chi}_{\omega,f}^{top}$ is a strictly increasing non continuous PL function with respect to e ; its discontinuity points are exactly the non-proper values of f .

Proof. The original curve $\gamma_{\omega,f}(e)$ is well-defined because $\sum w_i = 0$ [Dyn97]; since the Dynnikov indices of a pair saddle-center are opposite, the restricted sum $\sum_{top} w_i$ is still zero and therefore also $\gamma_{\omega,f}^{top}(e)$ is well defined.

Considering only the sum of the topological saddles is equivalent to cancel from a leaf all closed leaves that are homotopic to zero in \mathcal{M} , so that the averaged Euler characteristic now is only relative to the non-trivial closed leaves only.

Now consider a positive cylinder: since the values inside are smaller with respect to the values on the cylinder, the height of the cylinder increases with

e ; for the same reason, negative cylinders decrease their height. Since $\bar{\chi}_{\omega,f}^{top}(e) = \sum_{top} h_j^+ - \sum_{top} h_k^-$, then the function $\bar{\chi}_{\omega,f}^{top}(e)$ is strictly increasing in its continuity points. The function fails to be continuous when new pairs of topological saddles are created or destroyed, namely in the non-proper values of f , and it jumps exactly by the height of the cylinder(s) created or destroyed. \square

Corollary 2. *If ω induces on \mathcal{M}_e a Dynnikov decomposition of genus bigger than 1, then $e_1(\omega) = e_2(\omega) = e_0$, i.e. ω induces only closed leaves at any other level.*

Corollary 3. *At almost all levels of f the measure of the “ergodic” directions is zero.*

We have now all ingredients to prove theorem 4:

Proof. We will just discuss the case of “full ergodicity”, namely the case of directions giving rise to leaves dense on the whole polyhedron; the same line of arguments extends to the lesser ergodic cases.

If ω induces on \mathcal{M} fully ergodic leaves, then of course no cylinder can appear and therefore, for any Morse PL function f such that $\mathcal{M} = f^{-1}(0)$, it must happen that $\bar{\chi}_{\omega,f}^{top}(0) = 0$. Let us consider now $\bar{\chi}^{top}$ as a function of ω and e : then the surface $X = (\bar{\chi}_f^{top})^{-1}(0) \subset \mathbb{RP}^2 \times \mathbb{R}$, for a generic function f , is transversal to the sections $\mathbb{RP}^2 \times \{e\}$: indeed in a projective chart, say $h^z = 1$, we have that $\partial_{h^x} \bar{\chi}_{\omega,f}^{top} = \sum_i w_i (c_i^{top})^x$ and similarly for h^y , so that the points on X where the gradient is zero are exactly the points where $\gamma_{\omega,f}^{top}(e) = \sum_i w_i c_i^{top} = 0$. This condition is non-generic, that finally proves the claim of the theorem. \square

2.5 Structure of the Stereographic Map of surfaces and triply periodic functions

The results of the previous two sections show that the SM $\mathcal{S}(\mathcal{M})$ of a generic surface is the disjoint union of a countable set of open sets $\mathcal{D}_l(\mathcal{M})$ (“islands”), each labeled by a $l \in PH_2(\mathbb{T}^3, \mathbb{Z})$, immersed in a sea of directions that give rise only to closed leaves. According to our intuition of the system and the numerical experiments made to date, we conjecture that generically the number of islands is finite, but no rigorous proof of this fact exists. As matter of fact, this structure is exactly the one guessed, from symmetry consideration, by the physicist I.M. Lifschitz and his Karkov school about fifty years ago [LP59, LP60].

The boundaries of the islands are reached when the last pair of genus-1 components collide because of a cylinder collapse and therefore are characterized by the presence of (at least) a pair of inequivalent critical points on the same leaf. The set of these directions is the countable union of the curves $\langle \mathbf{H}, \hat{c}_i - \hat{c}_j \rangle = 0$, $i \neq j$; such curves in the polyhedra case are all straight lines, so that every island is actually a (not necessarily convex) polygon. There are reasons to believe that these polygons are convex for low genus, i.e. at least for genus 3 and 4, but it is easy to build examples of high-genus polyhedra with islands that are either

non connected or connected but non convex or even connected but non simply connected.

A crucial observation by Dynnikov [Dyn97] allows to associate a SM also to triply periodic functions:

Theorem 5. *Be f a Morse triply periodic function: then, if ω induces on \mathcal{M}_{e0} a Zorich decomposition \mathcal{Z}_{e0} , it induces a Zorich decomposition \mathcal{Z}_e for all $e \in (e_1(\omega), e_2(\omega))$ and all these decomposition share the same soul.*

Definition 11. *The island $\mathcal{D}_l(f)$ corresponding to the label l is the union of the corresponding islands of f 's level sets: $\mathcal{D}_l(f) = \cup_{e \in \mathbb{R}} \mathcal{D}_l(\mathcal{M}_e)$. The SM of f is the union of all its islands: $\mathcal{S}(f) = \cup_l \mathcal{D}_l(f)$*

The SM corresponding to functions are generically dramatically different from those corresponding to surfaces.

First of all, since rational directions induce necessarily Zorich decompositions, the set of islands $\mathcal{S}(f)$ is now always dense in \mathbb{RP}^2 , and of course lemma 2 also tells us that in this case the sea of directions giving rise to closed leaves only dried up, since every direction either belongs to an islands (or its boundary) or is ergodic.

Moreover, the following property shows that the islands can be sorted in a rather complex way:

Theorem 6. *Generically every two zones meet transversally and in a countable number of points.*

Proof. No point belonging at the same time to two different zones \mathcal{D}_{l_1} and \mathcal{D}_{l_2} can have irrationality degree bigger than 2, since it must contain the integer direction $l_1 \times l_2$. In the smooth case this would be enough, since the boundaries are smooth curves and they generically contain only a countable number of 2-irrational points and no rational point. In the PL case though the boundaries are actually segments of straight lines and therefore they are actually contained in the set of the directions with irrationality degree smaller than one.

Nevertheless, the theorem holds also in this case for the following reason: since every direction at the boundary between two zones is perpendicular to the direction $l_1 \times l_2$, then their set is the straight line (in \mathbb{RP}^2) passing through l_1 and l_2 . Generically none of the two labels falls on the boundary and therefore two zones can meet in a number of points not bigger than the number of sides of the island with the smaller number of sides. \square

Corollary 4. *Either there is a single zone, i.e. it exists a label l such that $\mathcal{D}_l(f) = \mathbb{RP}^2$, or there are countably many zones and they are dense in the whole projective plane.*

Since the islands meet trasversally, the non trivial SM will look like 2-dimensional Cantor sets. Retrieving numerically such fractals is not trivial since it involves, in general, to analyze the system at several values of f , but there is a class of interesting (non generic) cases in which it is actually enough to analyze a single level surface of f to get the entire fractal picture:

Theorem 7. *Be \mathcal{M} a polyhedron whose interior is equal to its exterior, modulo the group $G \simeq \mathbb{R}^3 \times \mathbb{Z}_2$ of translations and inversion of the three axes. Then $\mathcal{S}(\mathcal{M}) = \mathcal{S}(f)$ for any function having \mathcal{M} as (connected component of a) level set.*

Proof. By symmetry, we can build a function f such that $\mathcal{M} = f^{-1}(0)$ and that $f^{-1}(e)$ is equal to $f^{-1}(-e)$, modulo G . Since also the bundles of parallel planes are invariant by G , it turns out that for such an f the interval $I(\omega)$ of existence of open orbits relative to any 1-form ω is of the form $I(\omega) = [-a(\omega), a(\omega)]$ and therefore $0 \in I(\omega)$, $\forall \omega \in \mathbb{RP}^2$, i.e. at the zero level every ω induces open leaves. \square

In particular, all triply periodic functions f such that $f(c - x, c - y, c - z) = -f(x, y, z)$ belong to this class, and indeed the only fractals analyzed numerically to date are relative to this kind of functions.

Finally, we cite an important property that ties the set of all labels relative to the islands of the SM of a function with the set of ergodic direction [Leo04a, Leo05a]:

Theorem 8. *The closure of the set of all labels is the disjoint union of the set of all zones boundaries and the set of ergodic directions.*

3 A concrete case study

As pointed out in the previous section, to date a picture of the fractal has been numerically produced for only two functions, an analytical one and a piece-wise quadratic one [Leo04a].

The analytical one is $f(x, y, z) = \cos(2\pi x) + \cos(2\pi y) + \cos(2\pi z)$, invariant with respect to translations by integers $\Gamma = \mathbb{Z}^3 \subset \mathbb{R}^3$, that gives rise to genus-3 level surfaces in the range $(-1, 1)$ and spheres at every other non-critical level. This function represents the simplest non-trivial case possible from the topological point of view, since any triply periodic connected surface of genus smaller than 3 lies between two parallel planes and therefore the asymptotics of plane sections is easily found. Its zero level is rather special: it is known as the Schwarz primitive function (or plumber's nightmare) and was studied by Schwarz in 1890 as one of the first examples of triply periodic minimal surface.

From the computational point of view, $\mathcal{SP} = f^{-1}(0)$ has three important properties:

SP1 its interior is a translate of its exterior, so that $\mathcal{S}(\mathcal{SP}) = \mathcal{S}(f)$;

SP2 it is invariant with respect to the natural action of the tetrahedral group T_d on the unitary cube, so that the whole SM can be obtained, for example, extending by symmetry to the whole \mathbb{RP}^2 the data obtained for the triangle with vertices $[(0, 0, 1)]$, $[(1, 0, 1)]$ and $[(1, 1, 1)]$;

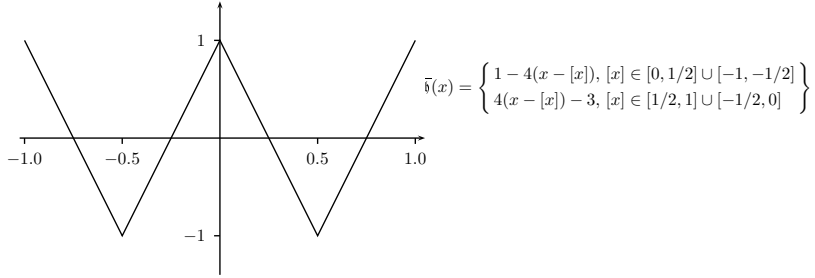


Figure 3: The simplest PL approximation of the cosine function.

SP3 the two cylinders, one negative and one positive, have the same height, so that it is enough to examine just one of the four topological critical points at the base of the two cylinders to retrieve all information about the structure of the foliation.

The piecewise quadratic function is $\mathfrak{g}(x, y, z) = \sum \bar{\mathfrak{g}}(x^i)$, where $\bar{\mathfrak{g}}$ is the simplest piecewise quadratic function having the same symmetries of the cosine function. Its level sets have the same behaviour as the function above but the expression of the critical points as function of the direction of the 1-form and the level of the function is so simple that allows a comparison between analytical and numerical data also at levels different from zero.

Nevertheless, in both cases the number of triangles needed to describe in sufficient detail the surface is so big (between 10^5 and 10^6) to make impossible to improve the resolution of the results obtained in [Leo04a], at least until a new algorithm is found or some “ad hoc” trick used.

3.1 The polyhedron

A natural way to improve the resolution of the numerical analysis of the problem is to consider PL functions, since in this case the number of triangles needed to describe their level surfaces can be as low as of the order of 10^1 . Moreover, the description of the surfaces is in this case exact rather than an approximation.

The simplest case to study, in order to take advantage of the extremely convenient properties evidenced in the \mathcal{SP} case, is the PL function $\mathfrak{h}(x, y, z) = \sum_i \bar{\mathfrak{h}}(x^i)$, where $\bar{\mathfrak{h}}$ is the function shown in Fig. 3. The polyhedron $\mathcal{P}_0 = \mathfrak{h}^{-1}(0)$ is a PL embedding of a genus-3 surface in \mathbb{T}^3 having 8 hexagonal faces, 20 edges and 12 vertices; the smallest triangulation for \mathcal{P}_0 takes $4 \cdot 8 = 32$ triangles, $32 \cdot 3/2 = 48$ edges and 12 vertices, that gives the expected Euler characteristic $\chi(\mathcal{P}_0) = F - E + V = -4 = 2 - 2 \cdot 3$. The basic cell of the lift $\bar{\mathcal{P}}_0 \subset \mathbb{R}^3$ in the unit cube is a truncated octahedron (Fig. 4); it is noteworthy to notice that, like its smooth analog, also this surface is, in the discrete sense, a minimal surface [Way04].

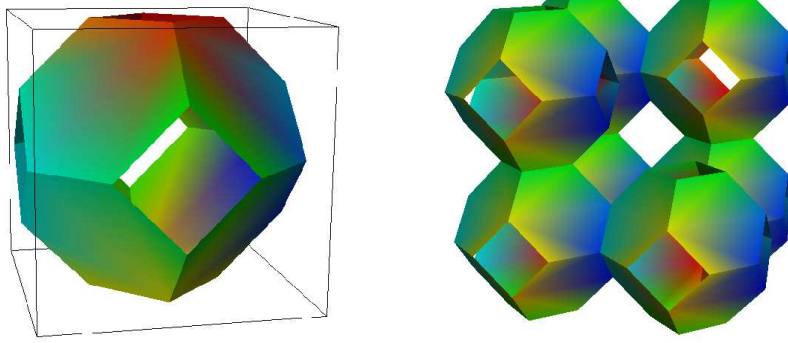


Figure 4: Plot of the Truncated Octahedron inside \mathbb{T}^3 (left) and of part of its image in the universal covering.

Since exactly four edges meet at every vertex, given any 1-form ω in general position with respect to \mathcal{P}_0 only saddles with index -1 may arise and therefore there are always four vertices that are critical for such ω . If the point p_1 is such a vertex, then the remaining three critical points are $p_{2,3} = (1/2, 1/2, 1/2) \pm p_1$ and $p_4 = (1, 1, 1) - p_1$. In particular in our numerical study we sample the set of 1-forms $\omega = (h^x, h^y, h^z)$ such that $h^x/h^z \in [0, 1]$ and $h^y/h^z \in [0, 1]$, for which the four critical points are $(0, .5, .75)$, $(.5, 1, 1.25)$, $(.5, 0, .25)$ and $(1, .5, .25)$.

3.2 The algorithm

In order to generate an approximate picture of the fractal, it is enough to produce an algorithm able to evaluate the label, if any, associated to a given 1-form. Since obviously no calculator can deal with irrational numbers, the numerical study will be limited to rational 1-forms; luckily this is not a big restriction, since anyway rational directions are dense in every stability zone.

Note that the algorithm used for the numerical study of the PL case is a simplified version of the more general algorithm we developed to study smooth surfaces of genus three [Leo04a], since in this case we know a priori the position of all critical points and moreover we know their position exactly, so that we do not have to correct “by hand” the topology of the critical section.

The basic idea to retrieve the label, as suggested to me by I. Dynnikov, is that the soul $l \in PH_2(\mathbb{T}^3, \mathbb{Z})$ associated to the Zorich decomposition \mathcal{Z} induced by $\omega \in \mathcal{D}_l$ is in 1-1 correspondance with the rank-2 sublattice of $H_1(\mathbb{T}^3, \mathbb{Z})$ obtained as the image, through the map $i_* : H_1(\mathcal{M}, \mathbb{Z}) \rightarrow H_1(\mathbb{T}^3, \mathbb{Z})$, of the open leaves in \mathcal{M} that have zero intersection number with the closed leaves populating the cylinders of \mathcal{Z} . Indeed, every cycle lying on the interior of a N_j component of \mathcal{Z} has no intersection with the closed leaves that form the cylinders \mathcal{C}_i , and since all N_j are homologous to each other (modulo sign) the

image of all these cycles in \mathbb{T}^3 must have rank-2; on the other side, there is an obvious 1-1 correspondance between rank-2 sublattices of $H_1(\mathbb{T}^3, \mathbb{Z}) = \Gamma \simeq \mathbb{Z}^3$ and the 2-tori embedded in $\mathbb{T}^3 = \mathbb{R}^3/\Gamma$, since every such 2-torus can be spanned by a pair of independent rational directions and viceversa.

The following algorithm **N** works for genus-3 polyhedra satisfying properties SP1-3, in particular for \mathcal{P}_0 :

Input: \mathcal{M} - the polyhedron; $\omega = (l, m, n) \in \mathbb{Z}^3$ - the 1-form; x - a critical point of ω with respect to \mathcal{M} ; $\pi_{\omega, x}$ - the plane perpendicular to (l, m, n) and passing through x .

Output: $c_{1,2}$ - the two critical loops²; $h_{1,2}$ - the homology classes of $c_{1,2}$ in \mathcal{M} ; $H_{1,2}$ - the homology classes of $c_{1,2}$ in \mathbb{T}^3 .

Algorithm:

- N1** retrieve the intersection between M and $\pi_{\omega, x}$;
- N2** check that there are exactly four critical branches and follow them by periodicity, otherwise exit;
- N3** if no other critical point is met along the path, so that the four branches are arranged in a pair of critical loops, store the two loops in the variables $c_{1,2}$, otherwise exit;
- N4** evaluate the homology class of $c_{1,2}$ in \mathbb{T}^3 and in M (this is actually done while executing N2 to speed up the computations time);
- N5** if the saddle is half-open, i.e. if exactly one among $H_{1,2}$ is zero, then associate to ω the complementary h triple, otherwise exit.

The main outcome of the algorithm is of course the label associated to ω . The fact that this label is a triple of integers is very important, since an integer evaluated numerically with an error smaller than .5 becomes actually an exact measure.

We implemented this algorithm in a C++ library named NTC³ built over an Open Source C++ library named VTK⁴. The choice of the language comes from the fact that VTK provides the basic geometric environment and algorithms needed by the problem, mainly the capability of generating meshes for isosurfaces and evaluating intersections between geometric objects. The inheritance mechanism of the C++ language allows to use transparently all functions of a library, hence we used VTK as a starting point and implemented in NTC the routines to deal with periodicity and evaluate the homology classes.

No serious attempt to evaluate the error on such calculations has been made to date since no need for it manifested. As check for the reliability of the result were rather used indirect evidences:

²since numerically we can study only the 1-rational case, in \mathbb{T}^3 the saddles are always wedges of circles, i.e. all critical branches close back to the critical point; according to whether these loops are or not homotopic to zero in \mathbb{T}^3 , their \mathbb{R}^3 lift will be open or close.

³<http://ntc.sf.net/>

⁴<http://www.vtk.org/>

- the agreement of the biggest zones with their analytical boundary (Fig. 7b), obtained through the independent algorithm **A**;
- the symmetry of the final picture with respect to the diagonal (Fig. 11), symmetry that was in no way used in the numerical calculations;
- the agreement of the fractal picture with the labels plot (Fig. 15).

The exploration of the SM was performed in the square $[0, 1]^2$ of the projective chart $(\omega_x/\omega_z, \omega_y/\omega_z)$ by evaluating the label associated to every direction at the vertex of a uniform grid of step r and it was repeated for the values $r = 10^2, 10^3, 10^4$. Samplings with $r = 10^2, 10^3$ have been successfully performed also for the previous two functions [Leo04a] but the CPU time needed to reach $r = 10^4$ in that case was way too big. It is because of the rather small number of triangles needed to describe \mathcal{P}_0 that the computation became doable.

3.3 Numerical results for $r = 10^2$

This resolution is the lowest one that allows to have a hint of the structure of the fractal. About r sections are needed to follow the critical branches for a generic direction (m, n, r) , $m, n \in \{1, \dots, r\}$, that takes a time of $.5s$ on a $1GHz$ CPU for the evaluation of a single label and $10^4 \times .5s \simeq 1h$ for sampling the 10^4 directions of the grid (Fig. 7).

Even from this rough picture it is rather evident a further symmetry of the picture, namely the one with respect to the antidiagonal of the square. This symmetry does not come, like the others, from the tetrahedral group T_d but it is rather of topological nature. The numerical evidence is that, if a 1-form (m, n, r) is labeled by L , then its symmetric $(1 - n, 1 - m, r)$ is labeled by $L + (1, 1, 0)$ but no proof of this fact is known.

In order to verify the correctness of the algorithm, we found “by hand” the analytical boundaries for the biggest zones and compared them with the numerical results (Fig. 7b). The following algorithm, aimed at the cases similar to the cosine one, is a slight modification of the original algorithm introduced and used by Dynnikov in [Dyn96]:

Algorithm A

- A1 fix a 1-form $\omega = (m, n, r) \in \mathbb{Z}^3$ inside some zone (e.g. extracting it from the experimental, guessing it from symmetry arguments or simply by trial and error);
- A2 retrieve the critical section of ω passing through one of its critical points c and make sure it is half open, otherwise exit;
- A3 evaluate the homology class l of the closed critical leaf C ;
- A4 rotate ω around some direction till the cylinder of which C is a base collapses and identify the critical point c' that is now connected to c through a saddle connection;

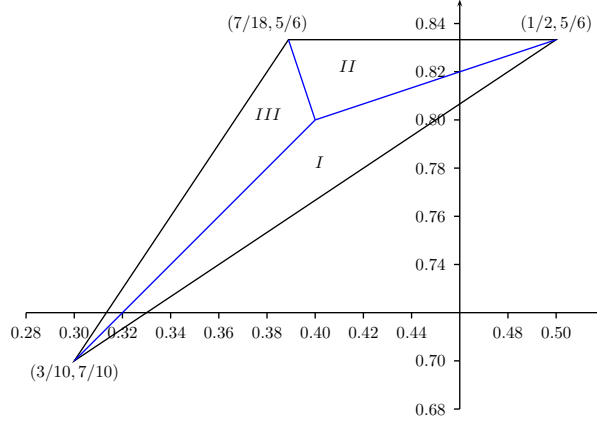


Figure 5: A close-up of the island $\mathcal{D}_{(2,4,5)}(\mathcal{P}_0) = \mathcal{D}_{(2,4,5)}(\mathfrak{h})$. Inside the island the pairs of critical points at the base of each cylinder are locally constant. In correspondance to each sides, there are three different pairings sorted in open subsets, labeled in the picture by roman numerals, separated by straight lines segments correspondng to directions ω for which the bases of the positive and negative cylinders collide, resulting in a saddle connection between two critical points. These three segments meet in the single point $(.4, .8)$, that in this case happens to be exactly the direction of the label (this property though is not generic). In Figure 6 we show in detail the transition between two different pairs within this island.

A5 the equation $\langle \mathbf{H}, c - c' \rangle = 0$ contains one of the sides of the island; follow it in one direction till four critical points fall over the critical closed leaf: this is the point when a sides and a new one start; repeat this step till the island boundary close up on themselves.

Since the genus is three, only two cylinders may appear and they will be of opposite sign. The pairs of critical points at the base of cylinders are locally constant; in the square under investigation the pairings are p_1, p_4 for the positive cylinder and p_2, p_3 for the negative one, so that boundaries are always given by an equation like $\langle \mathbf{H}, p_1 - p_4 + L \rangle = 0$. See Figures 5 and 6 for a concrete example worked out in detail.

Finally, a picture of the whole fractal can be obtained through the natural free action on \mathbb{RP}^2 of the tetrahedral group T_d , whose order is 24 (Fig. 7(d)).

3.4 Numerical results for $r = 10^3$

This is the highest resolution reached in [Leo04a]. In this case for each generic direction are needed about 10^3 sections to follow the critical branches, that takes a time of $2.5s$ on a $1GHz$ CPU for the evaluation of a single label and

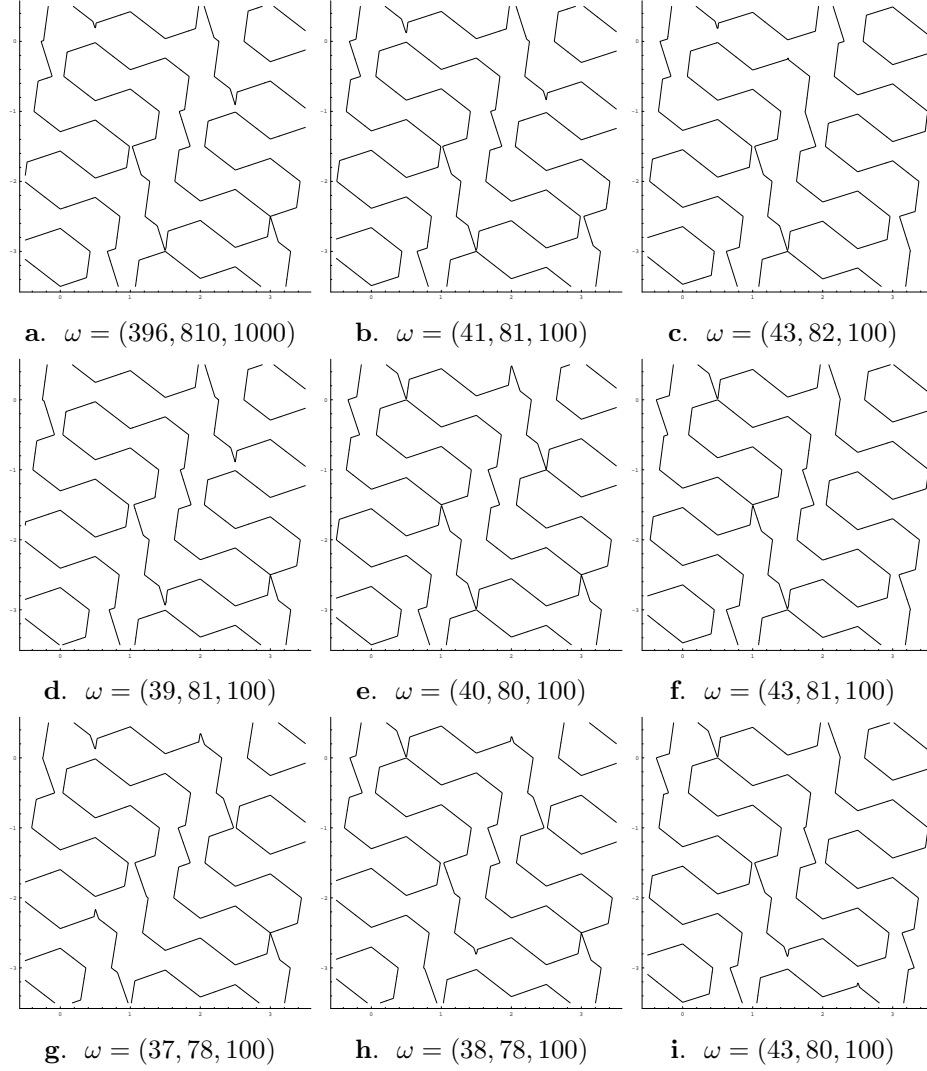


Figure 6: Significant examples of critical sections of \mathcal{P}_0 for $\omega \in \mathcal{D}_{(2,4,5)}(\mathcal{P}_0)$. At the “center” of the island (**e**) there is a saddle connection between the four critical points (starting from the highest and turning clockwise) $N = p_1$, $E = p_2 + (3, -3, 1)$, $S = p_1 + (1, -3, 2)$ and $W = p_2 + (1, -2, 1)$. In the subzones *I*, *II* and *III* (Fig. 5) the pairs of critical points at the base of the positive cylinder are, respectively, N and $p_4 + (2, -4, 1)$ (**i**), S and $p_3 + (2, -2, 0)$ (**b,c**) and E and $p_3 + (-1, -1, 0)$ (**d, g**). The separating segments correspond respectively to saddle connections between the pairs of critical points S and W (**a**), N and S (**f**) and N and E (**h**).

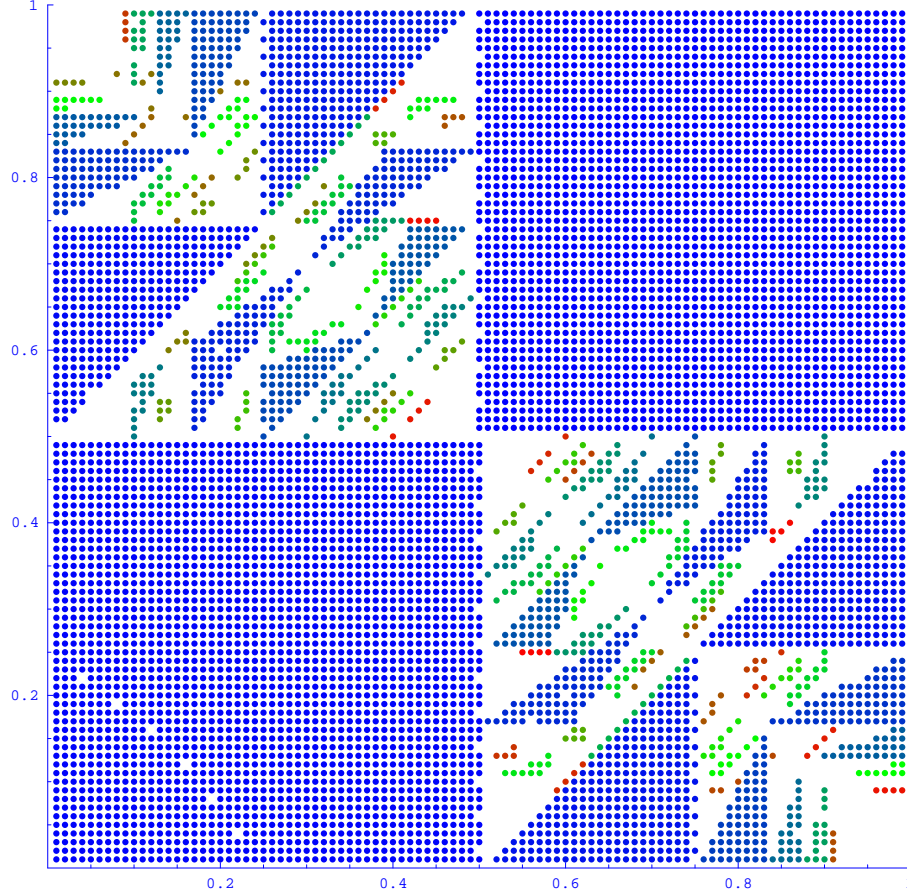


Figure 7: Numerical plot of the square $[0, 1]^2$ of the SM $\mathcal{S}(\mathcal{P}_0) = \mathcal{S}(\mathfrak{h})$ in the projective chart $h^z = 1$ at a resolution $r = 10^2$. The color of the islands goes from blue to red as the norm of the label grows. In the picture are displayed the 106 islands with at least four points out of the total 1741 islands found. The missing points that is possible to see in the interior of some of the islands are due to failure of the numerical algorithm **N**, e.g. because of the presence of saddle connections. The running time for the 10^4 steps cycle needed to retrieve these data takes about 1h on a Pentium 1GHz CPU.

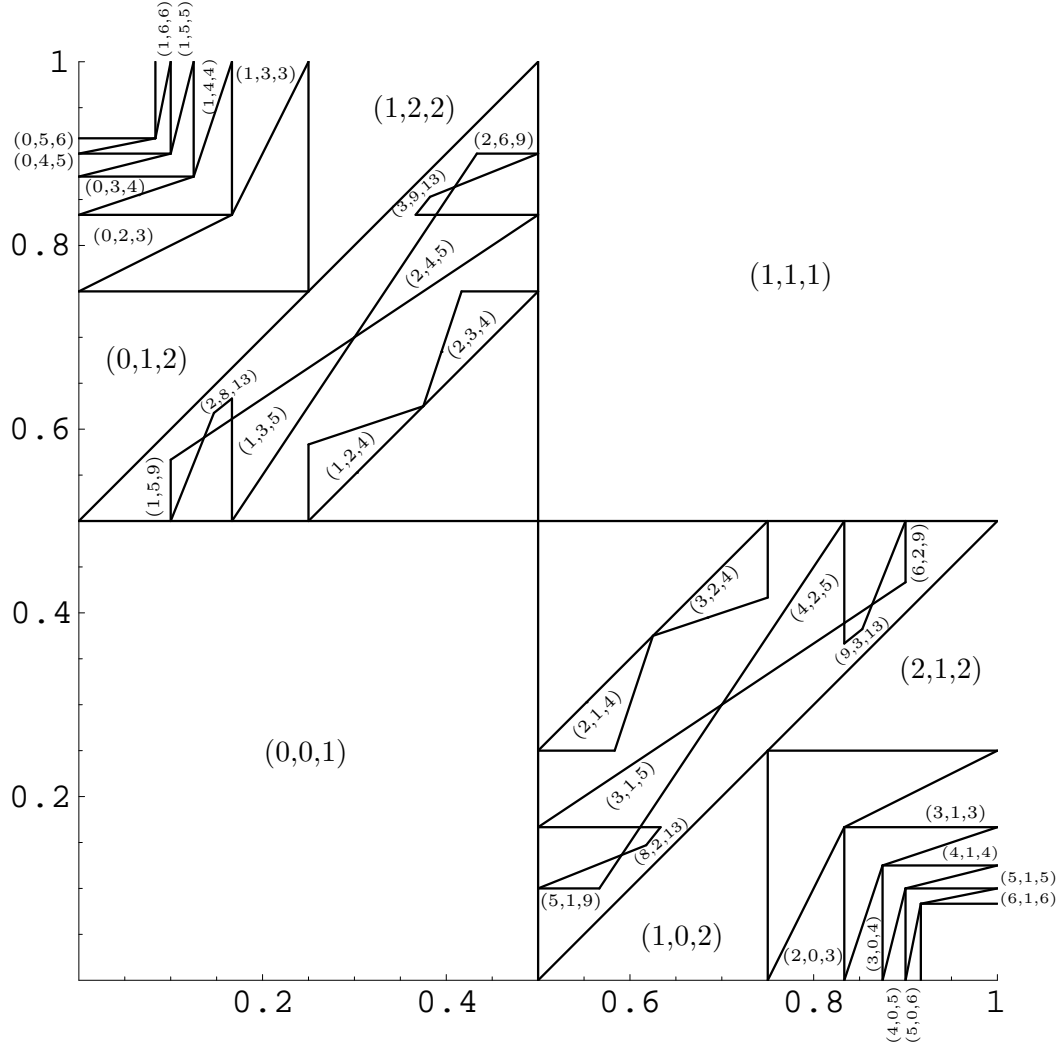


Figure 8: Analytical boundaries of the biggest islands found in Fig. 7 found using the algorithm **A**. All of their boundaries are straight lines segments and the corresponding label has been reported, when possible, inside the zone itself.

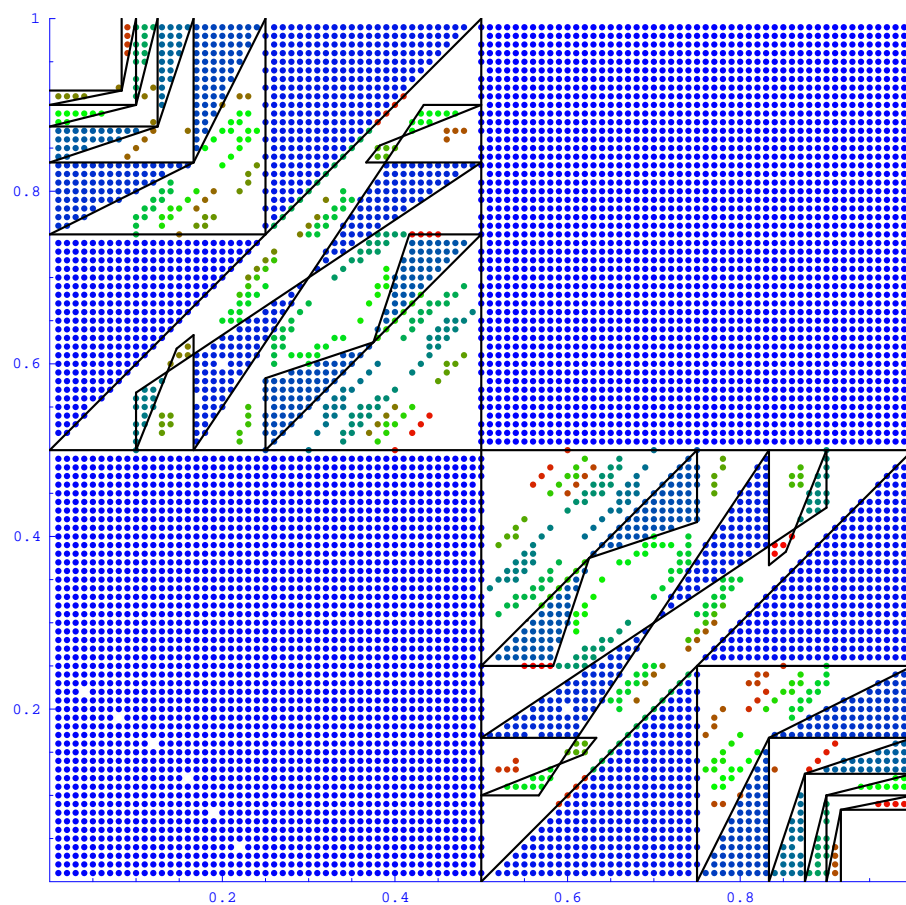


Figure 9: Comparison between analytical (Fig 8) and numerical (Fig 7) boundaries.

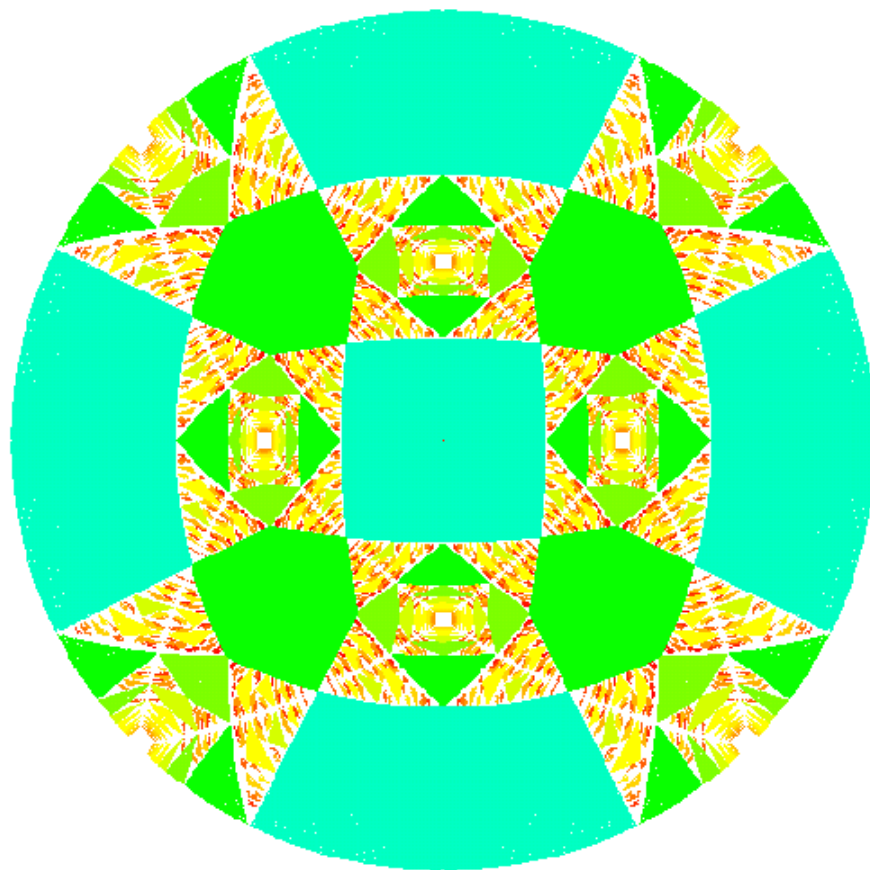


Figure 10: Fractal image obtained by letting the tetrahedral group T_d act on the square in Fig. 7 and then projecting on the disc through the stereographic map.

therefore about $5 \times 10^2 \times 1h \simeq 1month$ for sampling the 10^6 directions of the grid (Fig. 11).

A time of the order of a month is of course rather long, but thanks to the diffusion of the Linux OS, and therefore of the possibility to build big Unix clusters for cheap using PCs rather than workstations, this is still not too bad since it is easy to lower by a factor 10 the computations time just by dividing the cycle over as many PCs. This way the running time goes down to just three days, that is a rather acceptable time.

We point out that the situation is radically different in the smooth case: indeed in that case there is another variable to consider, that is the resolution of the mesh of the surface, that must be increased together with the grid resolution to avoid errors in the topology of the curve. The plane sections giving the complete intersection between the surface and a 2-torus with homology class (l, m, r) , $l, m \in [0, r]$, can be as close as $1/r$ and therefore, if the mesh is too rough, there is the risk that the program will jump on the wrong slice.

Concrete tests show that a mesh resolution of 30, meaning that the mesh is produced by dividing the unit cube in a 30^3 uniform grid, is enough for the $r = 10^2$ case but it must be raised to at least 60 for the $r = 10^3$ case, increasing the time for a single label evaluation to 15s, an order of magnitude bigger than in the PL case. This brings back the time to 3 months for the execution, that is indeed the order of the time spent for the $r = 10^3$ calculations made for [Leo04a].

From the picture 11 it is rather evident the symmetry with respect to the anti-diagonal. Apart from this, the picture looks qualitatively very similar to the pictures found in the previous two cases at the same resolution.

3.5 Numerical results for $r = 10^4$

Increasing by another order of magnitude the resolution, we increase by an order of magnitude the number of sections needed to follow a generic leaf, resulting in another factor 5 in the running time for a single evaluation of a 1-form label, that is now 10s, so that the total running time on a 1GHz CPU reaches $5 \cdot 10^2 \cdot 20d = 10^4d \simeq 30years$.

Such a big running time is rather scary and suggests that there is no hope to go up by an order of magnitude in resolution without changing some significant algorithm step. Nevertheless, this big time can be once again brought down to something reasonable by running the code in 20 PCs and by restricting the numerical analysis to the upper triangle of the square $[0, .5] \times [.5, 1]$ (that reduces computational time by a further factor 8). Thanks to all these expedients, the running time goes down by two orders of magnitude, reaching about 3 months, that is indeed about the time that took to us to collect the $r = 10^4$ data.

Note that for the smooth cases this would not be enough, since we must raise the mesh resolution to 10^2 and the time for the single evaluation goes up to 50s; this, together with the fact that there's a further factor two due to the lack of symmetry with respect to the antidiagonal, brings the total running time to 3 years, definitely not realistically affordable.

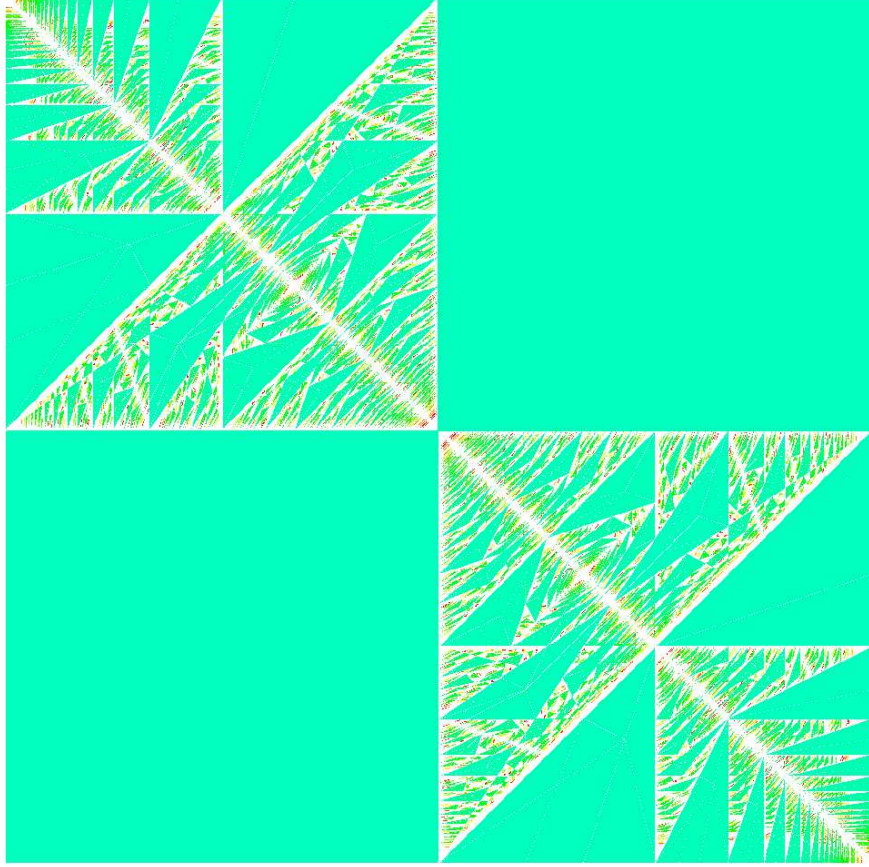


Figure 11: Numerical plot of the square $[0, 1]^2$ of the SM $\mathcal{S}(\mathcal{P}_0) = \mathcal{S}(\mathfrak{h})$ in the projective chart $h^z = 1$ at a resolution $r = 10^3$. The color of the islands goes from green to red as the norm of the label grows. In the picture are displayed the 1625 islands with at least four points out of the total 10725 islands found. The missing points that is possible to see in the interior of some of the islands are due to failure of the numerical algorithm **N**, e.g. because of the presence of saddle connections. The running time for the 10^6 steps cycle needed to retrieve these data takes about 1 week on a Pentium 1GHz CPU.

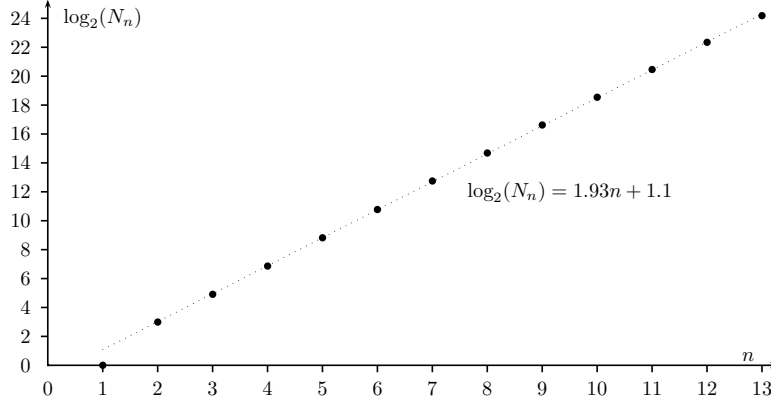


Figure 12: Box counting evaluation of the Hausdorff dimension of $\mathcal{S}(\mathcal{P}_0)$ with the $r = 10^4$ data. N_n is the number of squares of side 2^n needed to cover the complement of $\mathcal{S}(\mathcal{P}_0)$, the angular coefficient of the linear fit provides the dimension estimate. The same evaluation made with the $r = 10^3$ data gives a very close result, and also restricting the fit by canceling a few points at the extremes does not change considerably the estimate.

In Figures 17-30 are shown the numerical results, from which it is clear beyond any doubt that the SM has a fractal-like self-repeating structure, even though no explicit construction is known for it.

Numerical evaluations of the Hausdorff dimension $d_{\mathcal{P}_0}$ of the fractal set, namely the complement of $\mathcal{S}(\mathcal{P}_0)$ in \mathbb{RP}^2 , has been performed using the box counting technique (Fig. 12) and a sort of “area distribution” technique (Fig. 13).

The first, and more reliable, technique involves partitioning the square $[0, 1]^2$ in 2^n identical squares and evaluating the number of squares needed to cover the fractal. With the $r = 10^3$ data, n can get as big as $\log_2(10^3) \simeq 10$ and a linear fit gives an evaluation of $d_{\mathcal{P}_0} \simeq 1.93$. The $r = 10^4$ data allow n to go up to 13, representing the deeper results on the Hausdorff dimension of such fractals to date; figure 12 shows that the scaling law is linear to a high degree of accuracy and a linear fit gives again an estimate of $d_{\mathcal{P}_0} \simeq 1.93$, making us rather confident in the accuracy of this numerical result.

The second one involves counting the number of zones whose size is between b^n and b^{n+1} , where $b > 1$. Computations with several small values, between 2 and 1, were performed and all of them gives rough estimate of $d_{\mathcal{P}_0} \simeq 1.76$, further than expected from the evaluation given by the box counting. It is not clear to us the reason of this disagreement, that did not manifest for the smooth cases [Leo03], but it is not impossible that it may be due simply to the fact that this evaluation stabilizes at higher resolutions and therefore this evaluation is at the current state of things more or less unreliable (as simple numerical tests

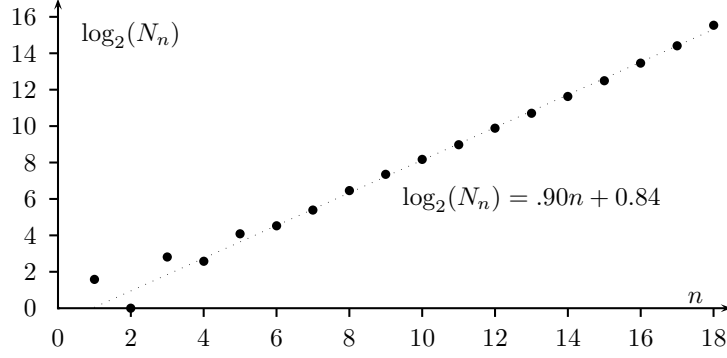


Figure 13: “Area distribution” evaluation of the Hausdorff dimension of $\mathcal{S}(\mathcal{P}_0)$ with the $r = 10^4$ data. N_n is the number of islands whose area is between 2^{-n} and 2^{-n-1} . The estimate of the Hausdorff dimension is given by the double of the angular coefficient of the linear fit and varies by ± 0.2 by restricting even by little the number of points on which the fit is made.

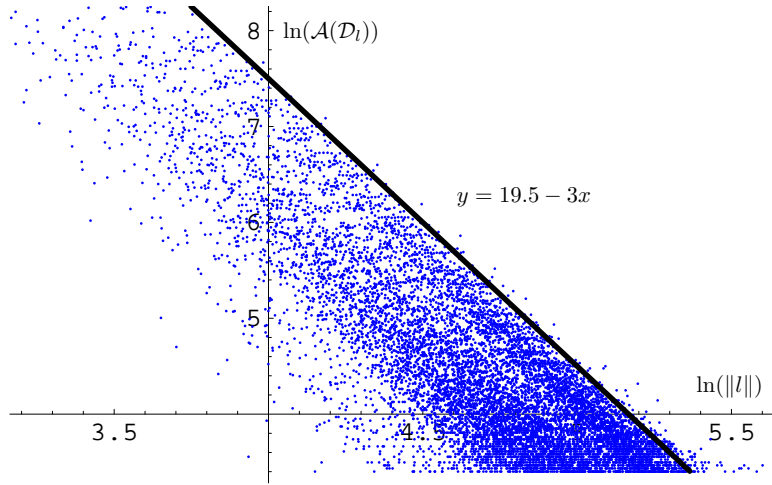


Figure 14: Logarithmic plot of the islands' areas versus the norm of the corresponding label. There is a very good agreement between the numerical data and the Dynnikov conjecture claiming that $\mathcal{A}(\mathcal{D}_l) \leq C/\|l\|^3$.

testify).

Finally, the $r = 10^4$ data provide enough detail to test numerically a conjecture by Dynnikov [Dyn99] and give a graphical evidence of theorem 8. The Dynnikov conjecture claims that the area of the islands satisfy a relation $\mathcal{A}(\mathcal{D}_l(\mathcal{M})) \leq C/\|l\|^3$ for some positive real number C depending only on the polyhedron \mathcal{M} ; the numerical data suggests that the exponent 3 cannot be improved any further (see Fig. 14).

According to theorem 8, the closure of the set of labels of $\mathcal{S}(\mathcal{P}_0)$, seen as points of \mathbb{RP}^2 , is equal to the complement of the interior of the islands. At this resolution about $5 \cdot 10^5$ different labels are found and their image in \mathbb{RP}^2 (Fig. 15) is one of the best indirect checks of correctness of the library NTC.

4 Conclusions

We proved in this paper that the structure of foliations induced on triply periodic embedded polyhedra by constant 1-forms is identical to the one induced on smooth surfaces, and we believe that the same line of arguments can also be used to further generalize the theorems to embedded piecewise smooth surfaces. This fact extends to “Morse PL functions” the association of a SM; in the most interesting cases such SM have a fractal nature (this condition is true for an open subset of all triply periodic PL functions, e.g for all triply periodic functions close enough to \mathfrak{h}).

Surfaces satisfying property SP1 (see section 3) are particularly rich, their SM being equal to the SM of any function having them as level set. We exploited this fact by studying the case of the triply periodic surface \mathcal{P}_0 obtained extending in the three coordinate directions a truncated octahedron. The simplicity of the triangulation of the surface allowed us to improve by an order of magnitude, respect to the results obtained in [Leo04a], the resolution of the numerical analysis of the fractal and, as a consequence, to perform several numerical tests on conjectures and theorems.

5 Acknowledgments

We want to thank first of all S.P. Novikov for introducing the subject. We are also deeply in debt with S.P. Novikov and I.A. Dynnikov for their interest in our work and for several precious and fruitful scientific suggestions and discussions that were essential for the present work. In particular, we thank I.A. Dynnikov for suggesting the analytical algorithm to retrieve the islands boundaries. All numerical calculations were made with computers kindly provided by the INFN section of Cagliari (www.ca.infn.it) and CRS4 (www.crs4.it). We also acknowledge financial support from the Cagliari section of INFN and from the Departments of Physics and of Mathematics of the University of Cagliari.

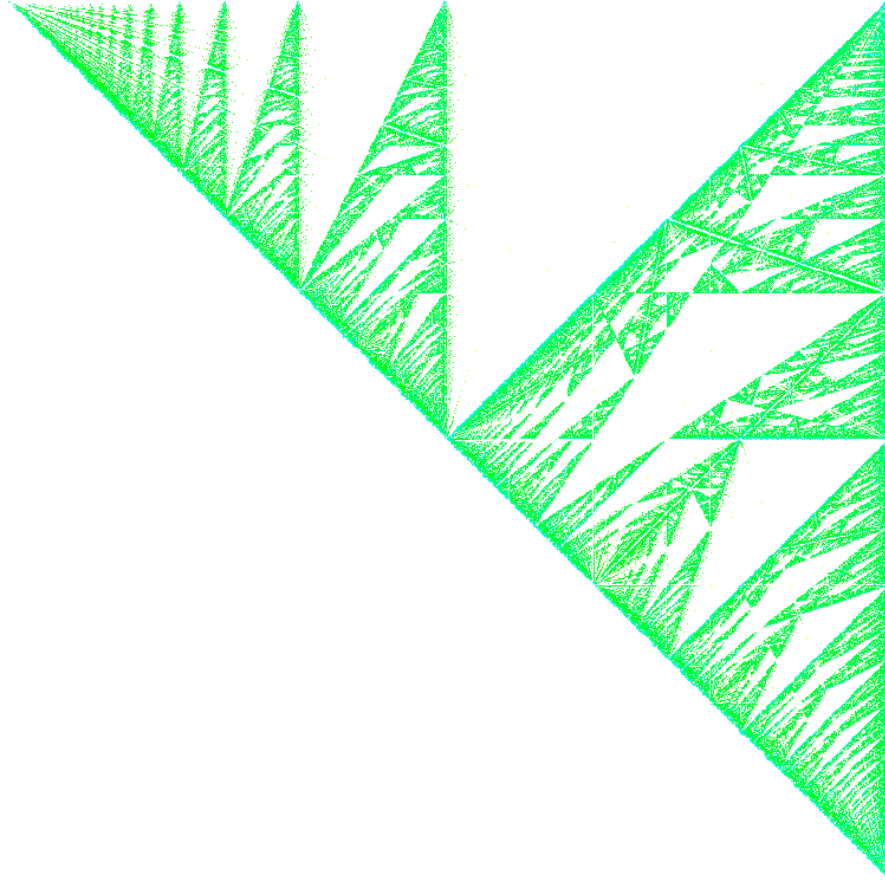


Figure 15: Plot of the labels of the 494041 islands found in the numerical analysis, at the resolution $r = 10^4$, of the portion of the SM $\mathcal{S}(\mathcal{P}_0)$ contained in the triangle of vertices $(0, 1)$, $(.5, 1)$ and $(.5, .5)$ in the projective chart $h^z = 1$. According to theorem 8, the closure of the set of labels is equal to the complement of the interiors of the islands; the striking closeness of the two pictures is one of the best indirect tests of the correctness of the implementation of the **N** algorithm in our C++ library NTC.

References

- [Ban67] T. F. Banchoff. Critical points and curvature for embedded polyhedra. *J. of Differential Geometry*, 1:245–256, 1967.
- [Ban70] T. F. Banchoff. Critical points and curvature for embedded polyhedral surfaces. *Amer. Math. Monthly*, 77:475–485, 1970.
- [Dyn92] I.V. Dynnikov. *Usp. Mat. Nauk (RMS)*, 57:3:172, 1992.
- [Dyn96] I.V. Dynnikov. Surfaces in 3-torus: geometry of plane sections. *Proc. of ECM2, BuDA*, 1996.
- [Dyn97] I.V. Dynnikov. *AMS Transl*, 179:45–73, 1997.
- [Dyn99] I.V. Dynnikov. *RMS*, 54:1:21–60, 1999.
- [Leo03] R. De Leo. Numerical analysis of the novikov problem of a normal metal in a strong magnetic field. *SIADS*, 2:4:517–545, 2003.
- [Leo04a] R. De Leo. Characterization of the set of “ergodic directions” in the novikov’s problem of quasi-electrons orbits in normal metals. *RMS*, 58:1042–1043, 2004.
- [Leo04b] R. De Leo. Topological effects in the magnetoresistance of au and ag. *Physics Letters A*, 332:469–474, 2004.
- [Leo05a] R. De Leo. First-principles generation of stereographic maps for high-field magnetoresistance in normal metals: an application to au and ag. *to appear on Physica B*, 2005.
- [Leo05b] R. De Leo. Proof of a dynnikov conjecture on the novikov problem of plane sections of periodic surfaces. *to appear on RMS*, 2005.
- [LP59] I.M. Lifschitz and V.G. Peschanskii. *JETP*, 8:875, 1959.
- [LP60] I.M. Lifschitz and V.G. Peschanskii. *JETP*, 11:137, 1960.
- [NM98] S.P. Novikov and A.Ya. Maltsev. *Usp. Fiz. Nauk*, 41:3:231–239, 1998.
- [Nov82] S.P. Novikov. *Usp. Mat. Nauk (RMS)*, 37:5:3–49, 1982.
- [Way04] R. Wayne. Infinite periodic discrete minimal surfaces without self-intersections. *arXiv:math/0410314*, 2004.
- [Zor84] A.V. Zorich. *Usp. Mat. Nauk (RMS)*, 39:5:235–236, 1984.

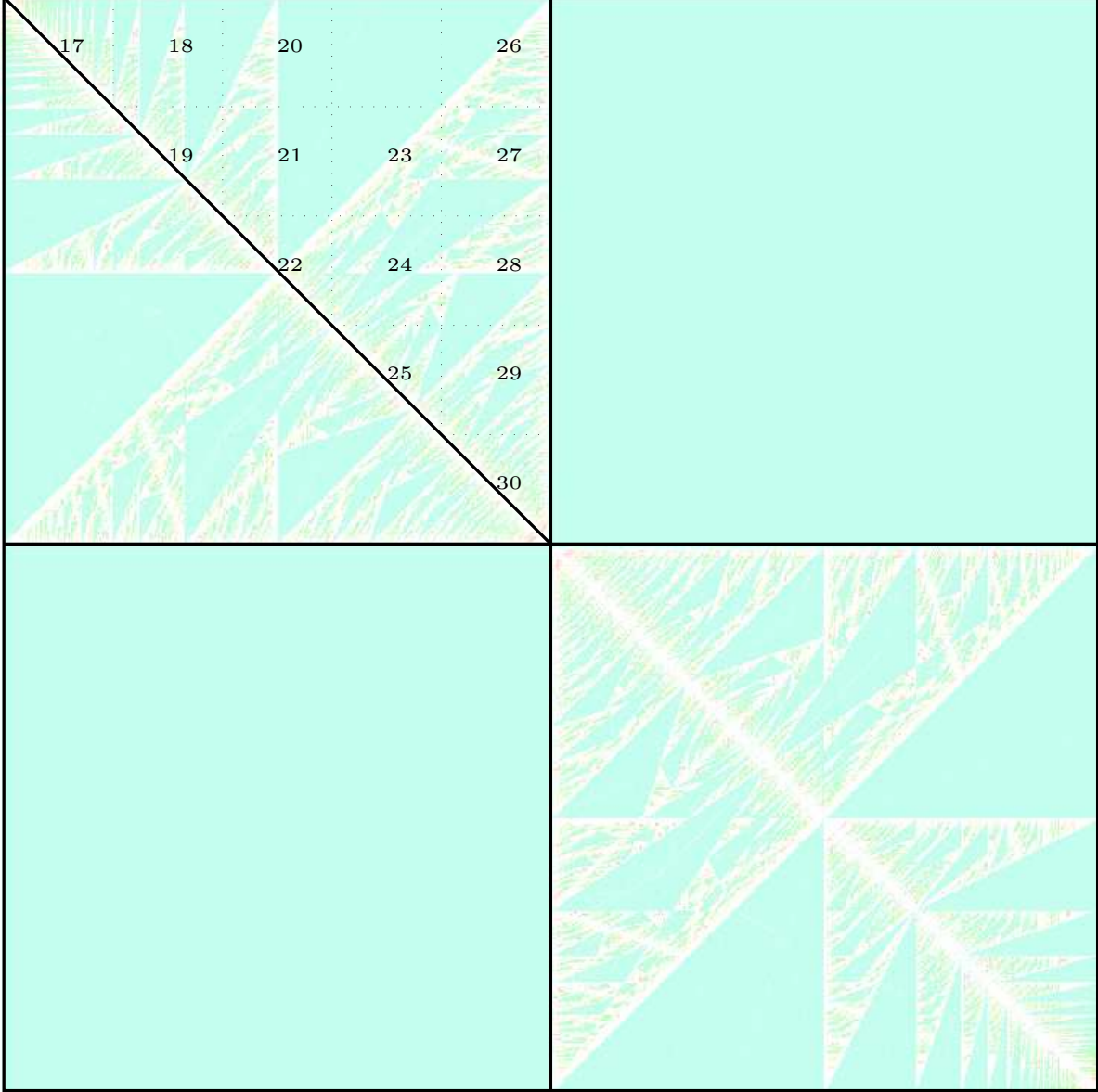


Figure 16: The next 14 pictures show, in full detail, the fractal structure of $\mathcal{S}(\mathcal{P}_0) = \mathcal{S}(\mathfrak{h})$ sampled at the resolution $r = 10^4$. In order to minimize the CPU time, the numerical analysis was limited to the triangle $[(0, 1, 1)]$, $[(1/2, 1, 1)]$ $[(1/2, 1/2, 1)]$, divided above in smaller squares and triangles by a uniform grid and labeled by the corresponding figure number; the full picture can be retrieved by applying the “topological” symmetry characteristic of this surface, namely the symmetry with respect to the antidiagonal, and then the 24 symmetries coming from the action of the tetrahedral group T_d . To retrieve these data we used about 20 1GHz Pentium III CPUs for about 3 months. In all pictures, the color of the islands goes from green to red as the norm of the label grows. Note that the square $[.4, .5] \times [.9, 1]$ is fully contained inside the island $\mathcal{D}_{(1,2,2)}$ and therefore its picture will not be shown.

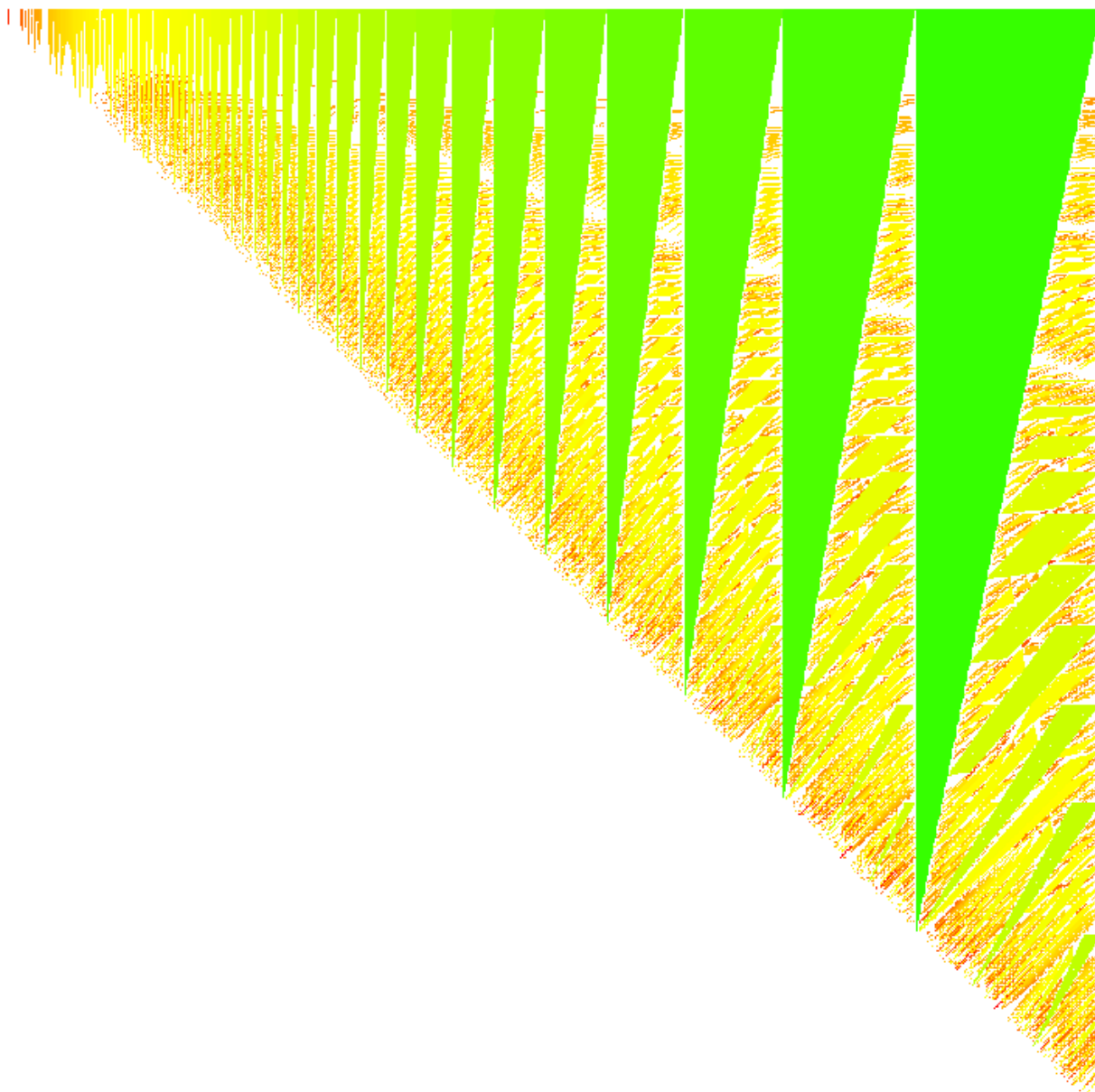


Figure 17: Detail of $\mathcal{S}(\mathcal{P}_0)$ in $[0, .1] \times [.9, 1]$

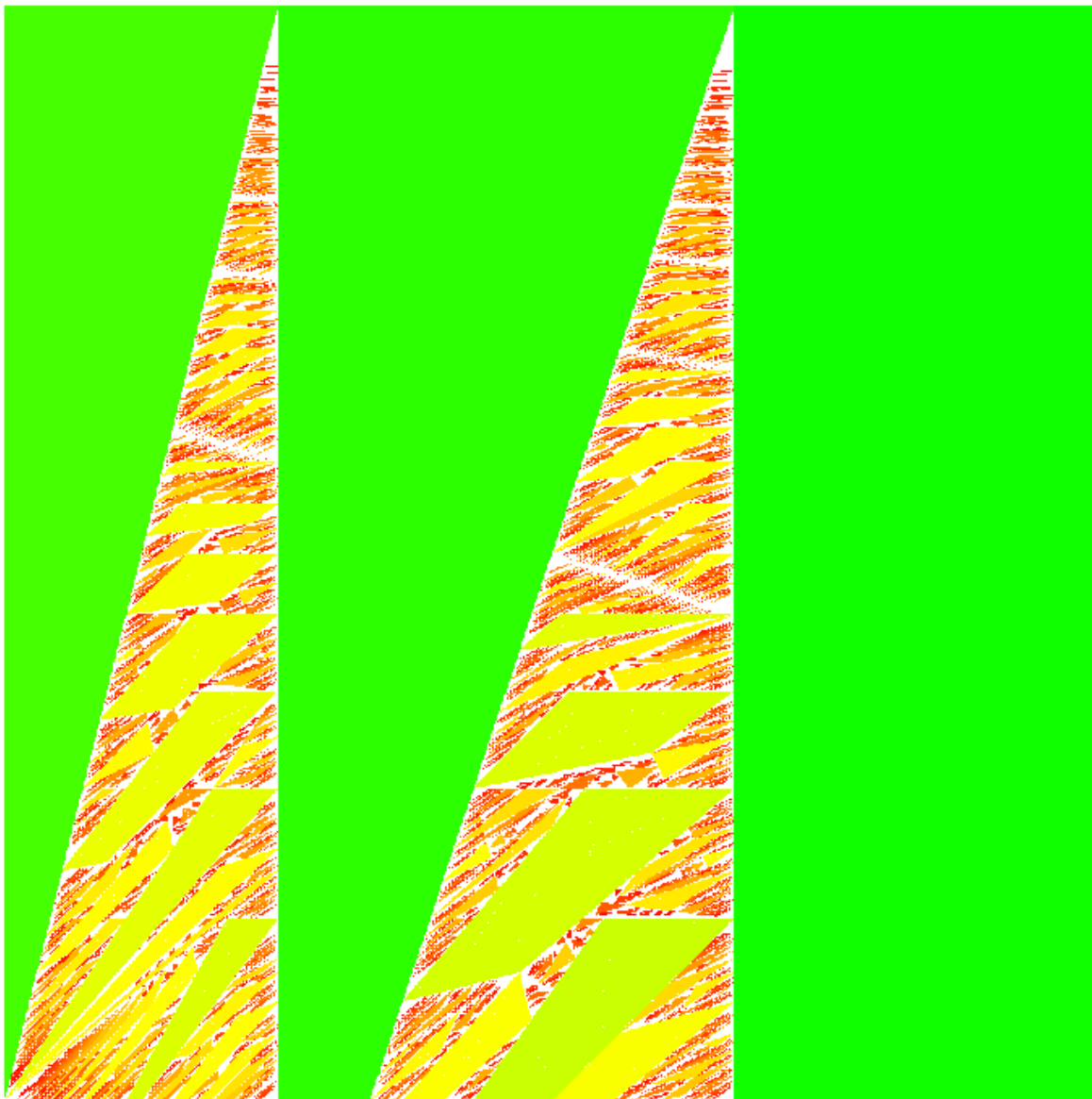


Figure 18: Detail of $\mathcal{S}(\mathcal{P}_0)$ in $[.1, .2] \times [.9, 1]$

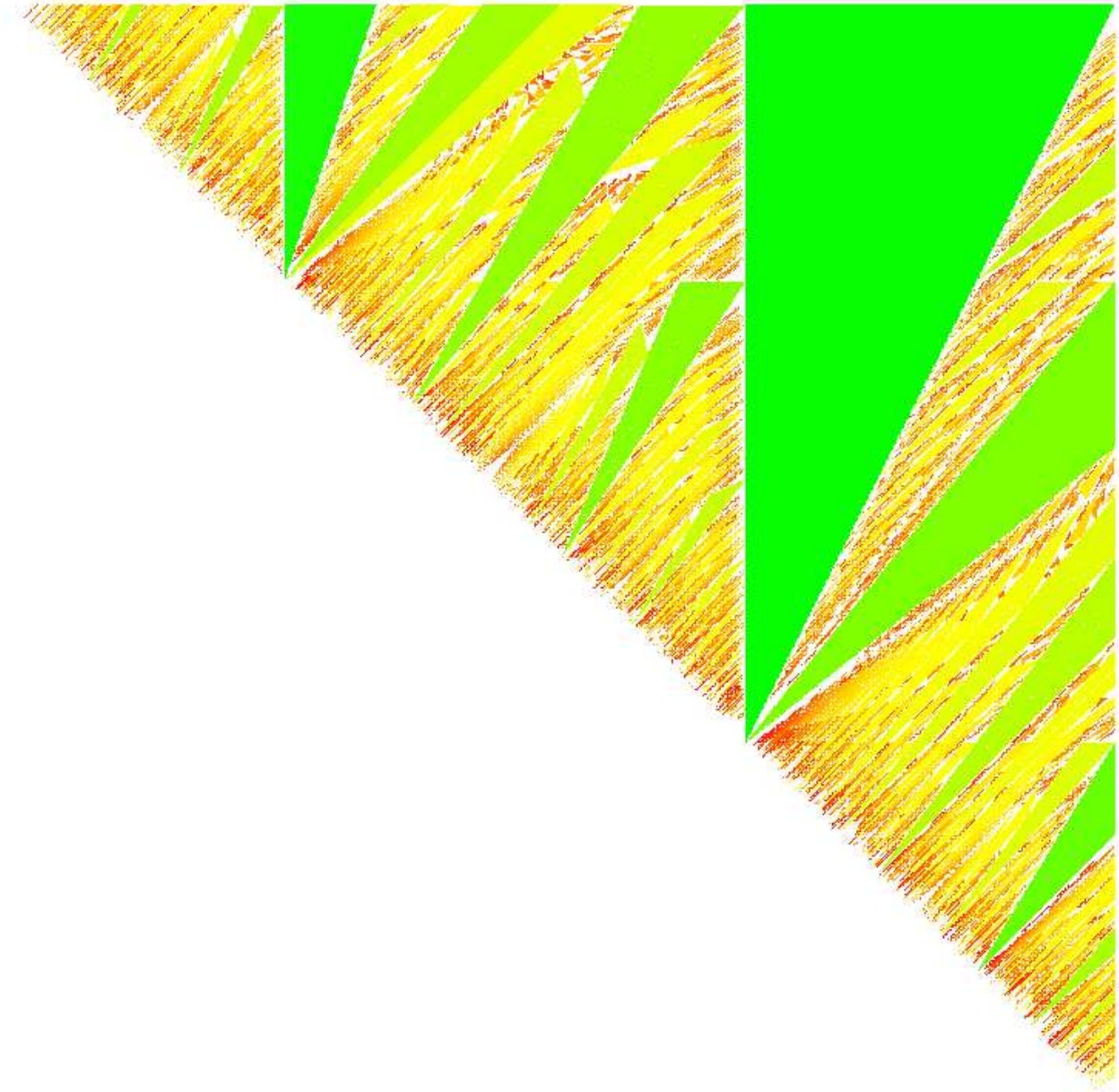


Figure 19: Detail of $\mathcal{S}(\mathcal{P}_0)$ in $[.1, .2] \times [.8, .9]$

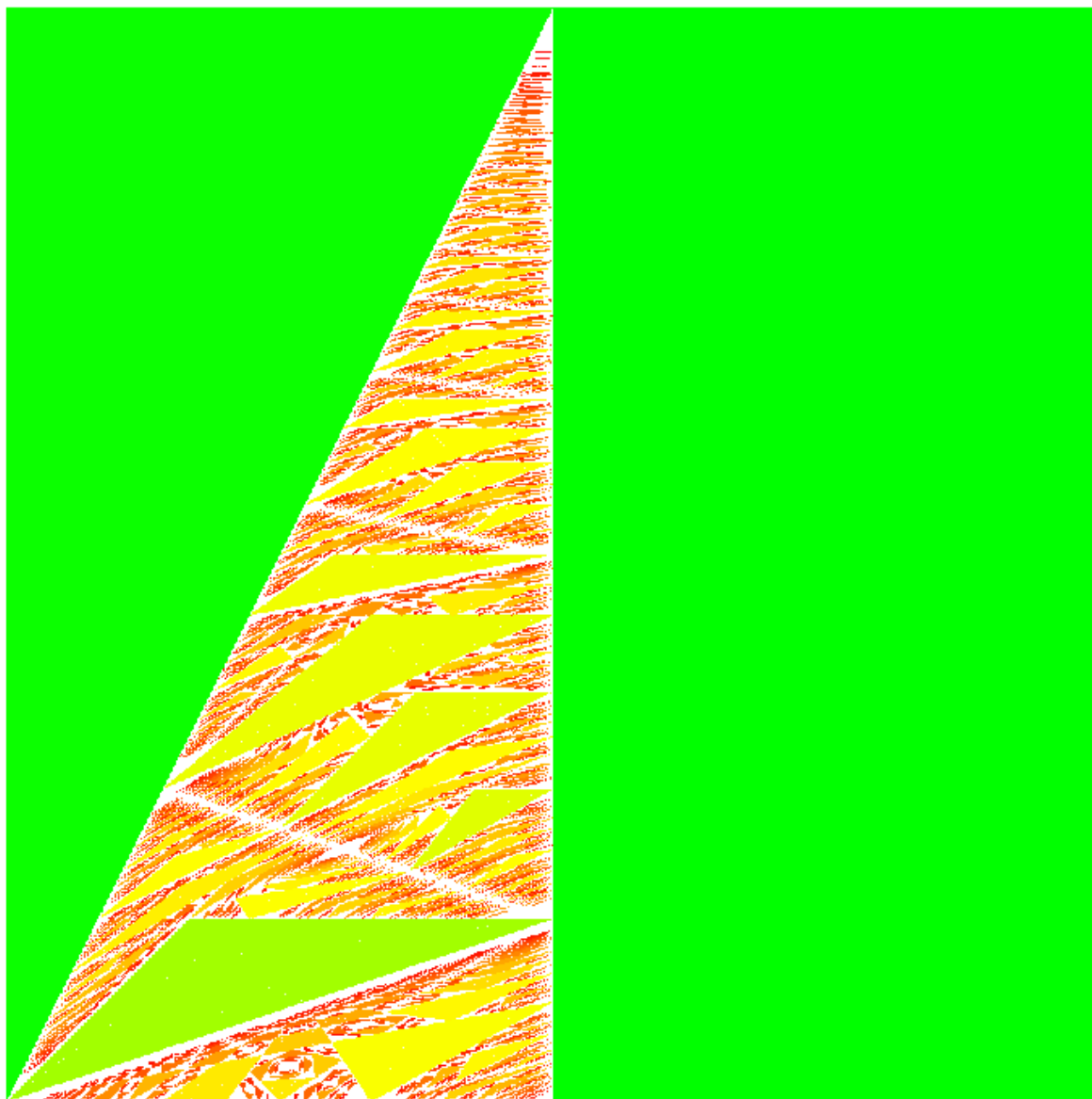


Figure 20: Detail of $S(\mathcal{P}_0)$ in $[.2, .3] \times [.9, 1]$

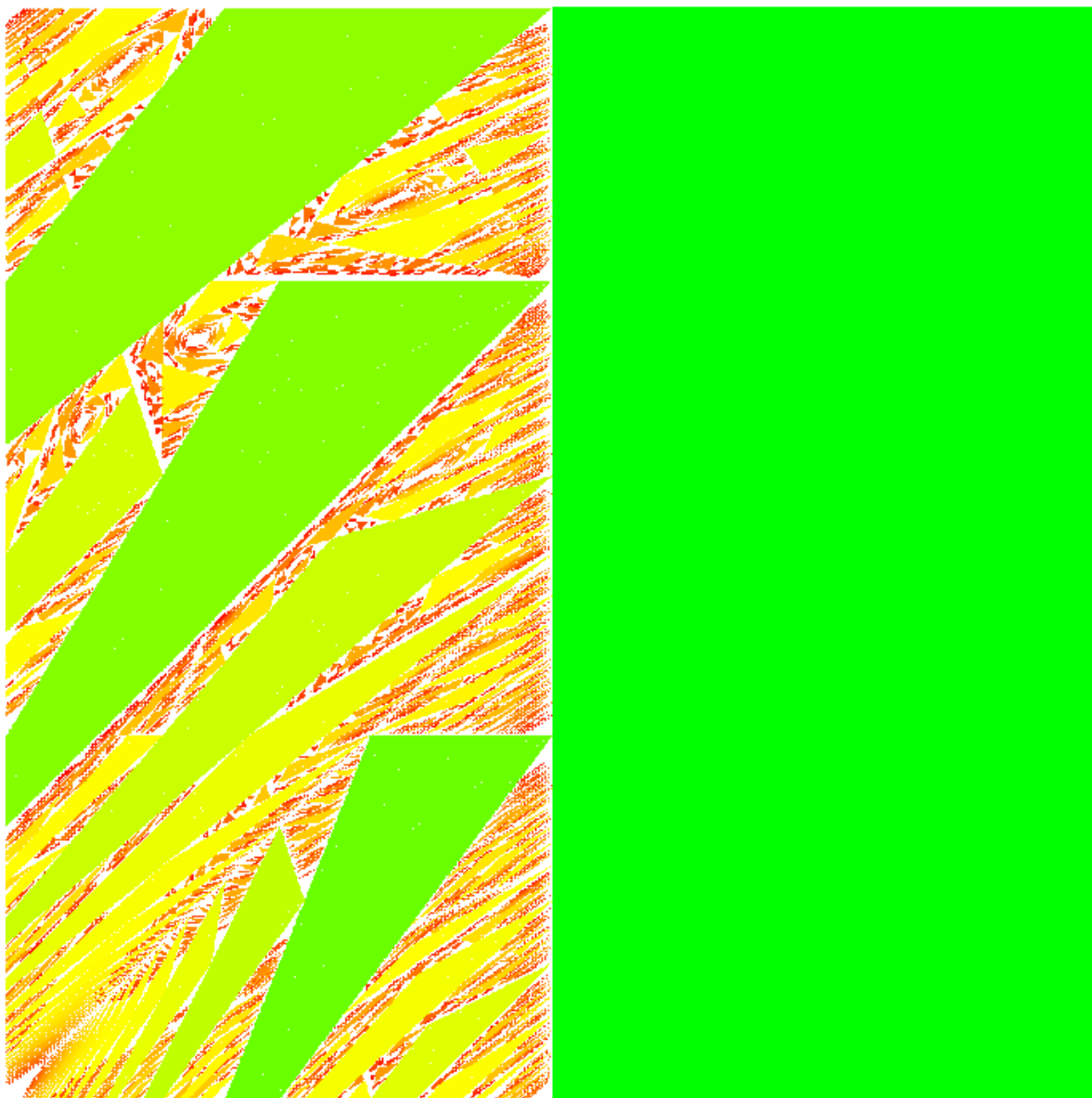


Figure 21: Detail of $\mathcal{S}(\mathcal{P}_0)$ in $[.2, .3] \times [.8, .9]$

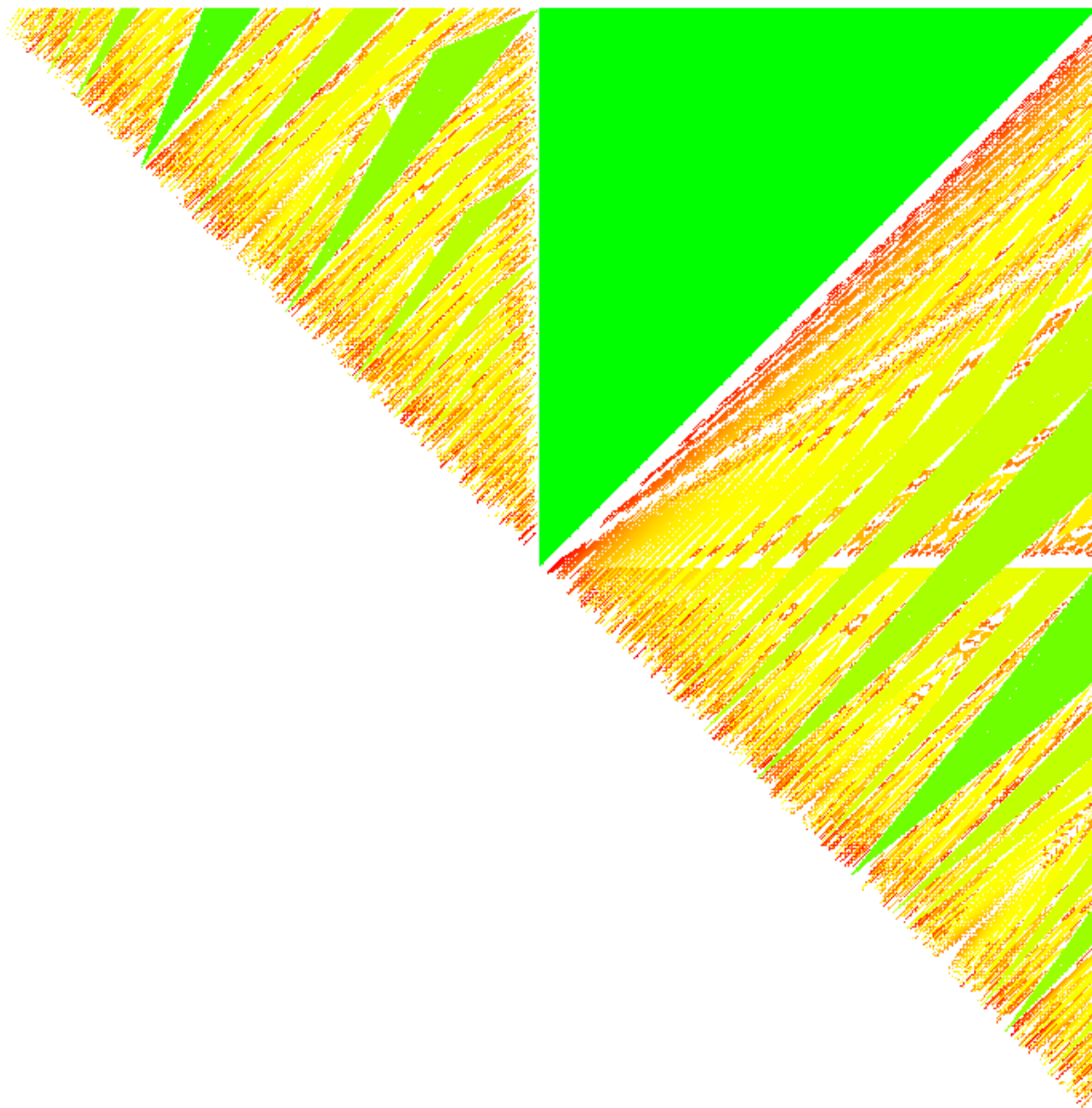


Figure 22: Detail of $\mathcal{S}(\mathcal{P}_0)$ in $[.2, .3] \times [.7, .8]$

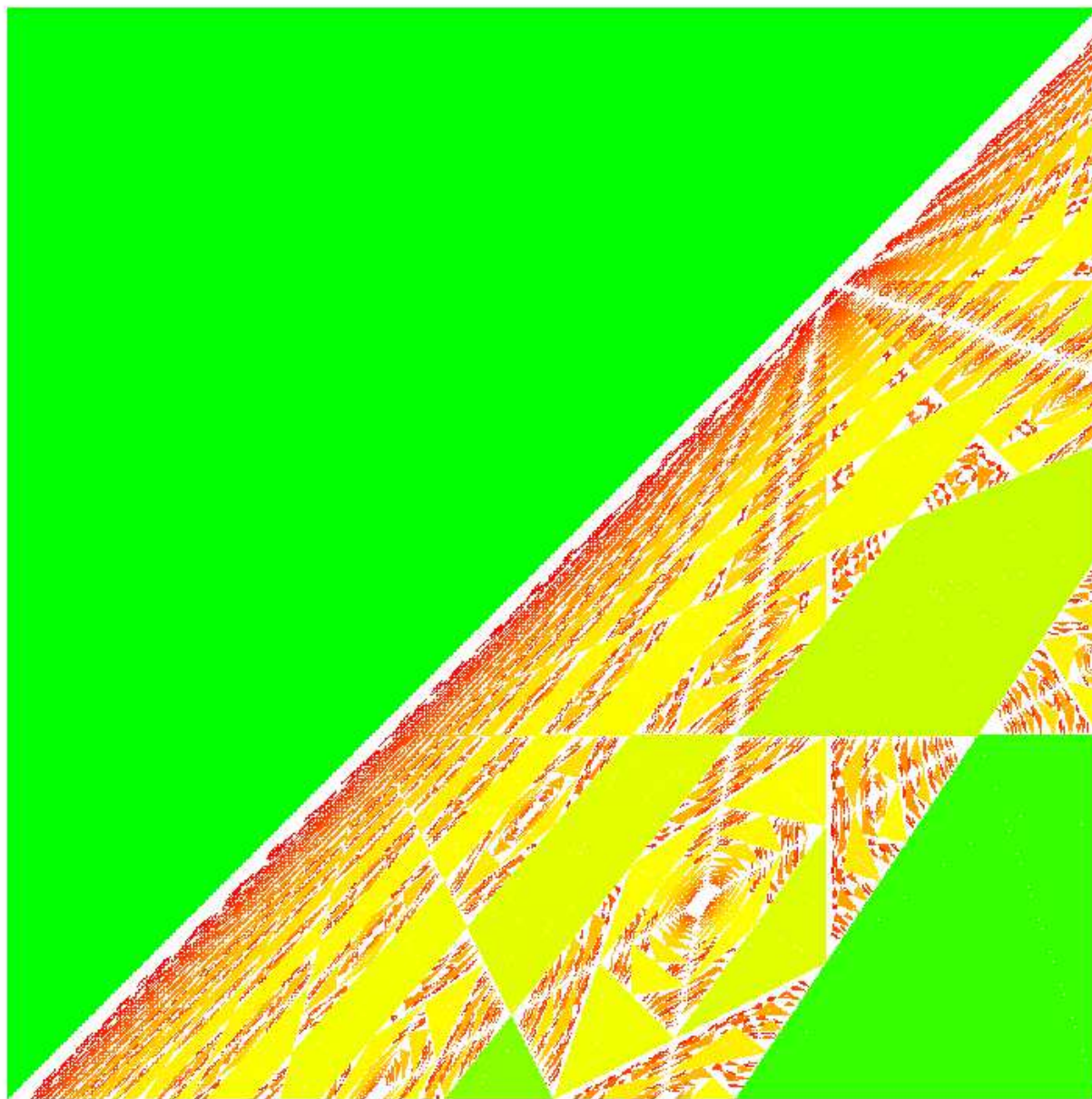


Figure 23: Detail of $\mathcal{S}(\mathcal{P}_0)$ in $[.3, .4] \times [.8, .9]$

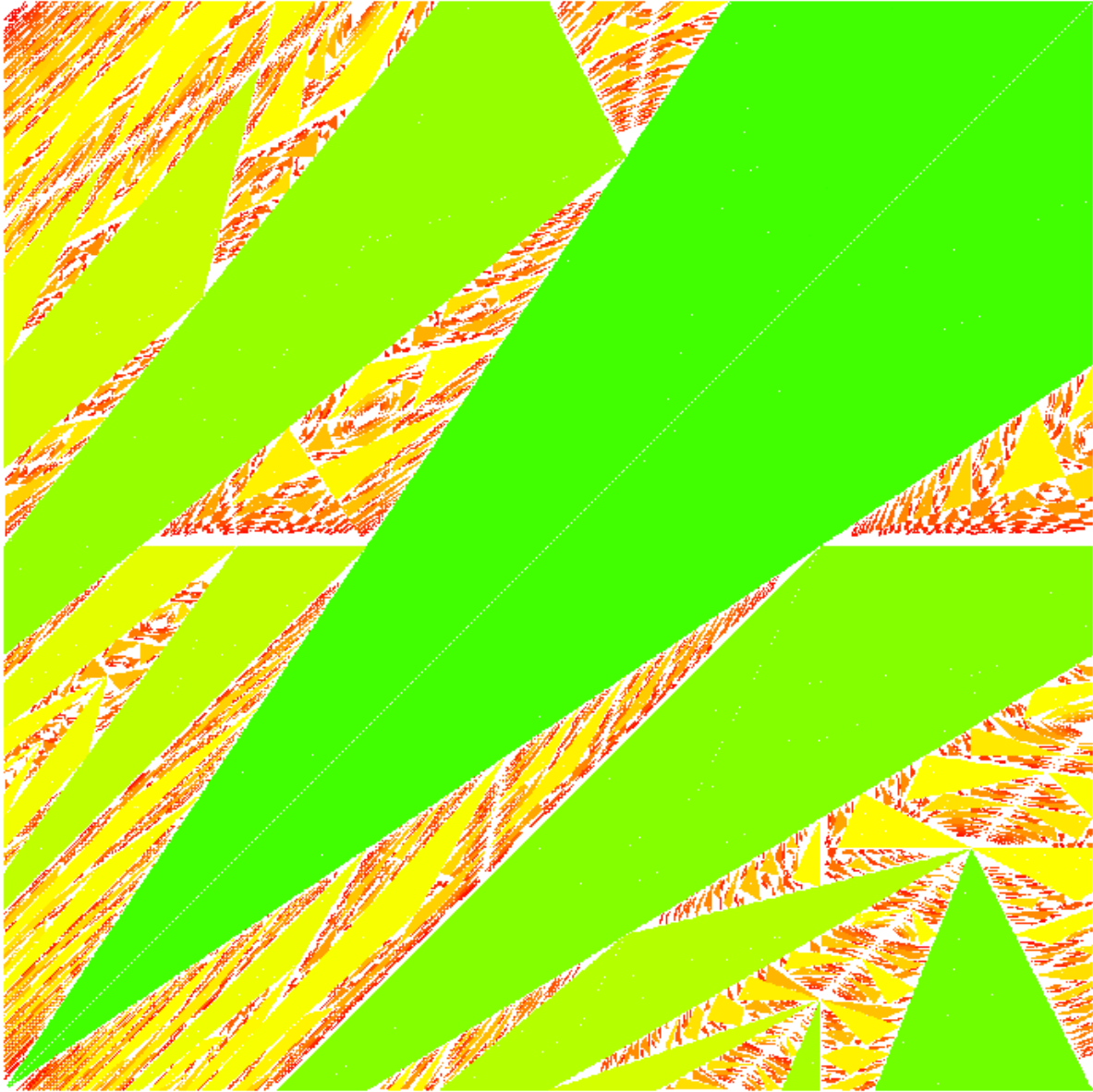


Figure 24: Detail of $\mathcal{S}(\mathcal{P}_0)$ in $[.3, .4] \times [.7, .8]$

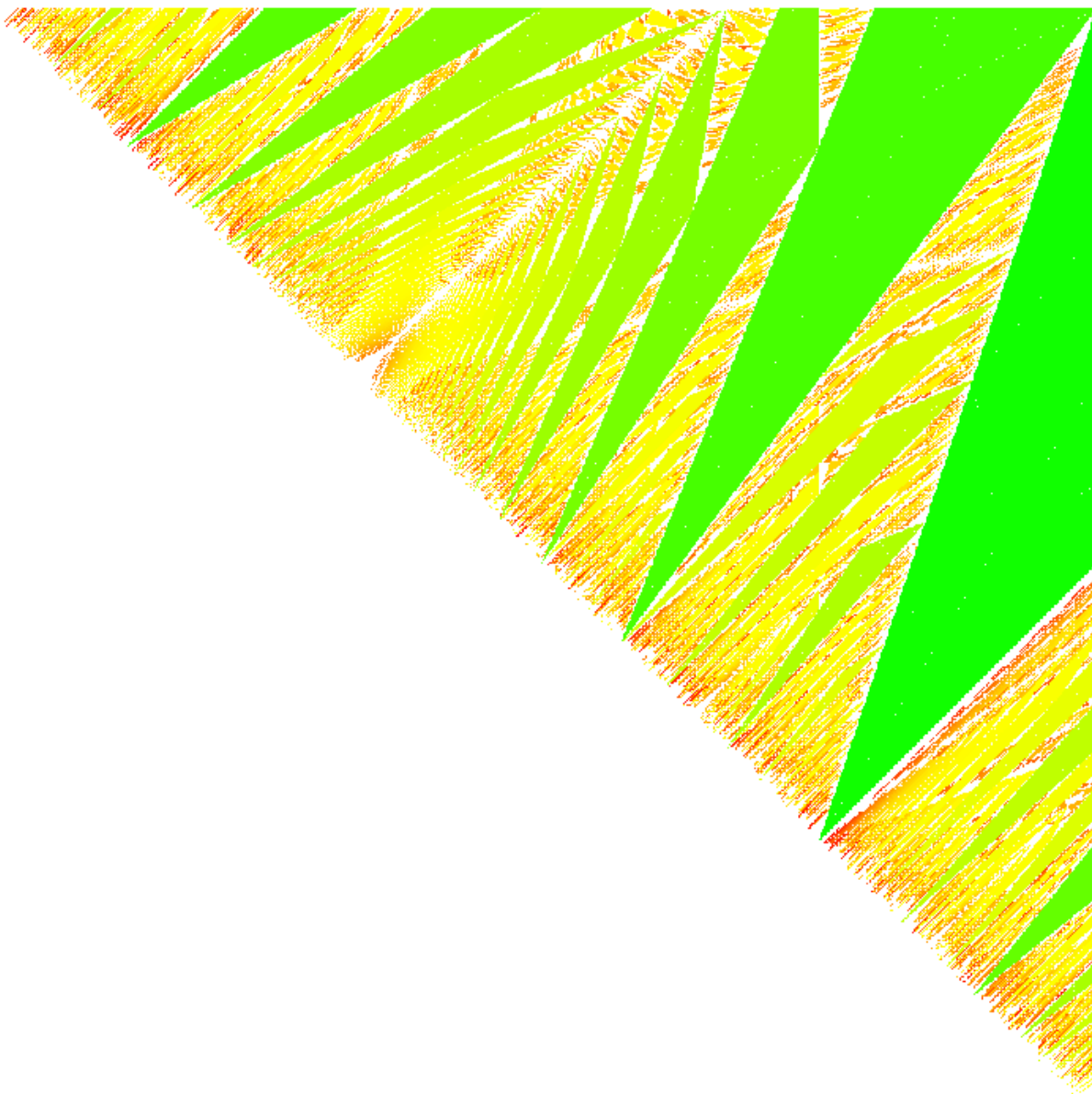


Figure 25: Detail of $\mathcal{S}(\mathcal{P}_0)$ in $[.3, .4] \times [.6, .7]$

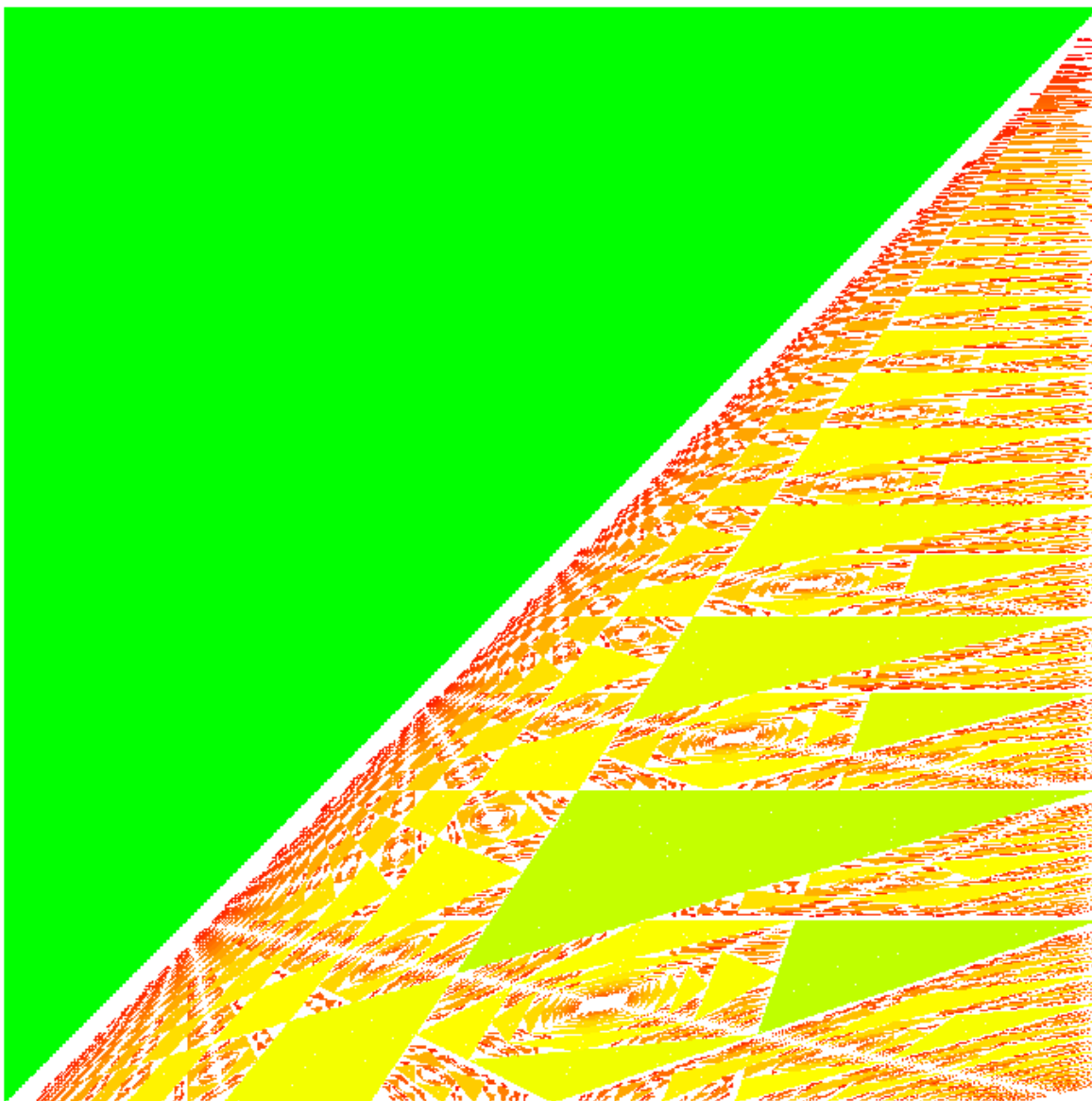


Figure 26: Detail of $\mathcal{S}(\mathcal{P}_0)$ in $[.4, .5] \times [.9, 1]$

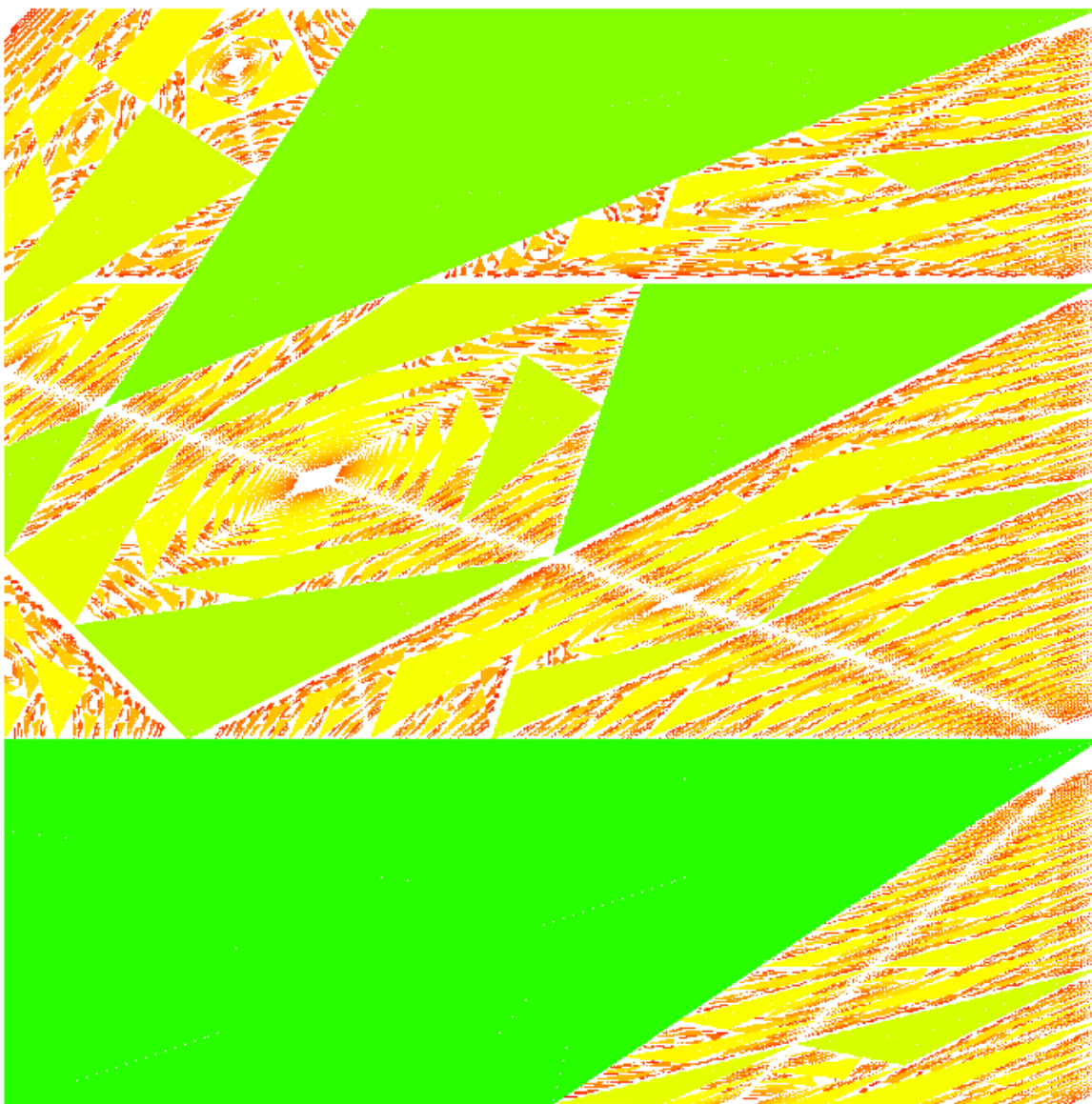


Figure 27: Detail of $\mathcal{S}(\mathcal{P}_0)$ in $[.4, .5] \times [.8, .9]$

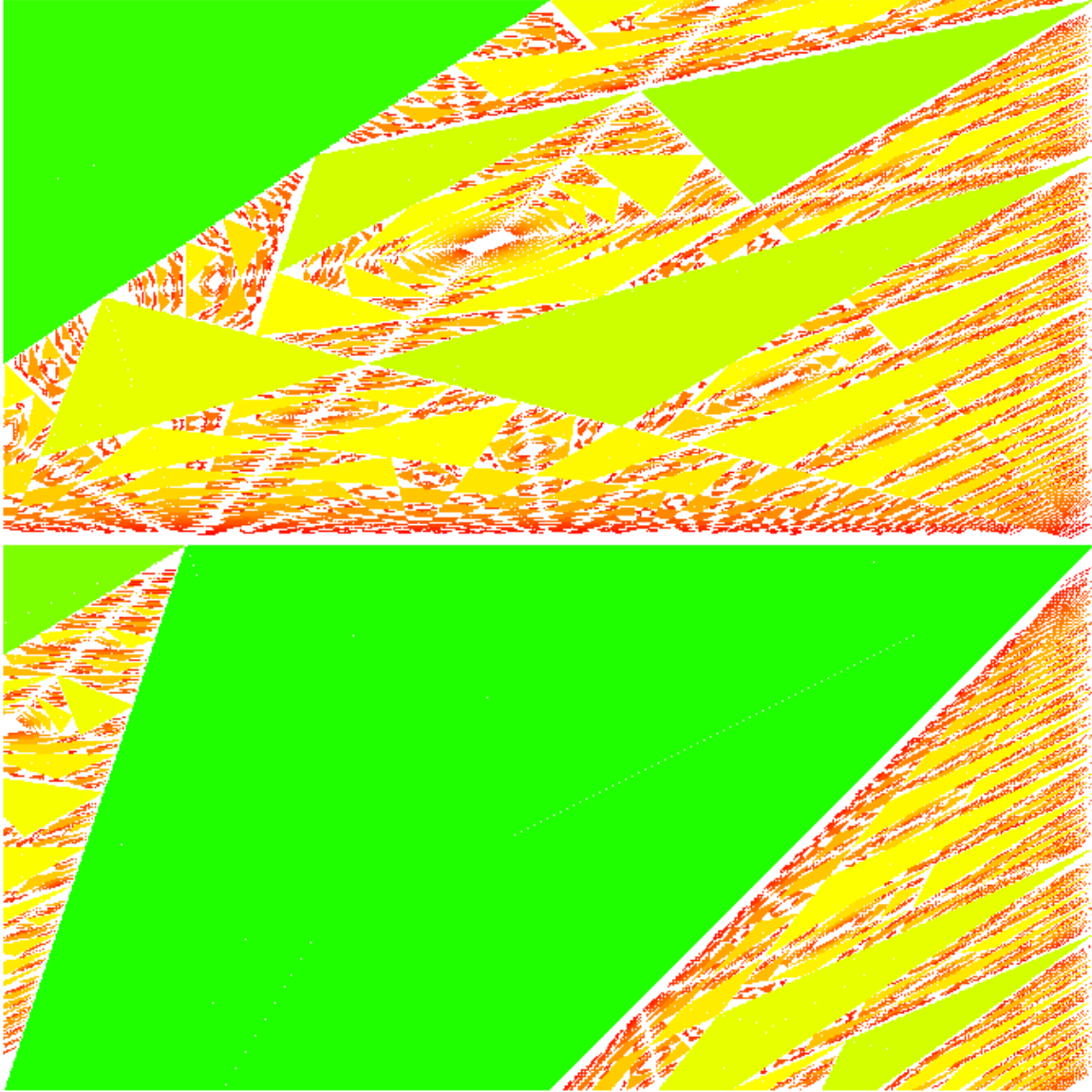


Figure 28: Detail of $\mathcal{S}(\mathcal{P}_0)$ in $[.4, .5] \times [.7, .8]$

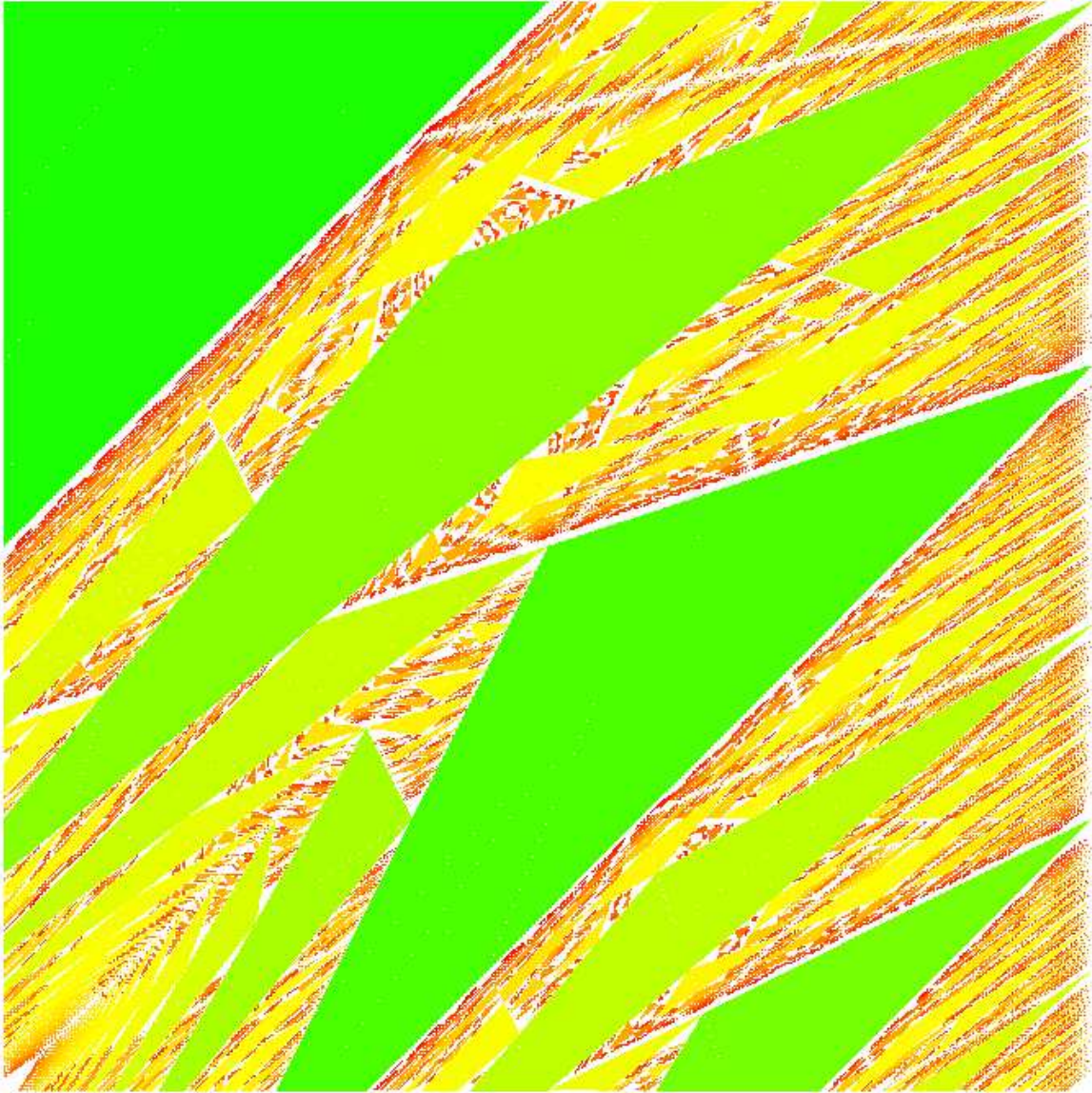


Figure 29: Detail of $\mathcal{S}(\mathcal{P}_0)$ in $[.4, .5] \times [.6, .7]$

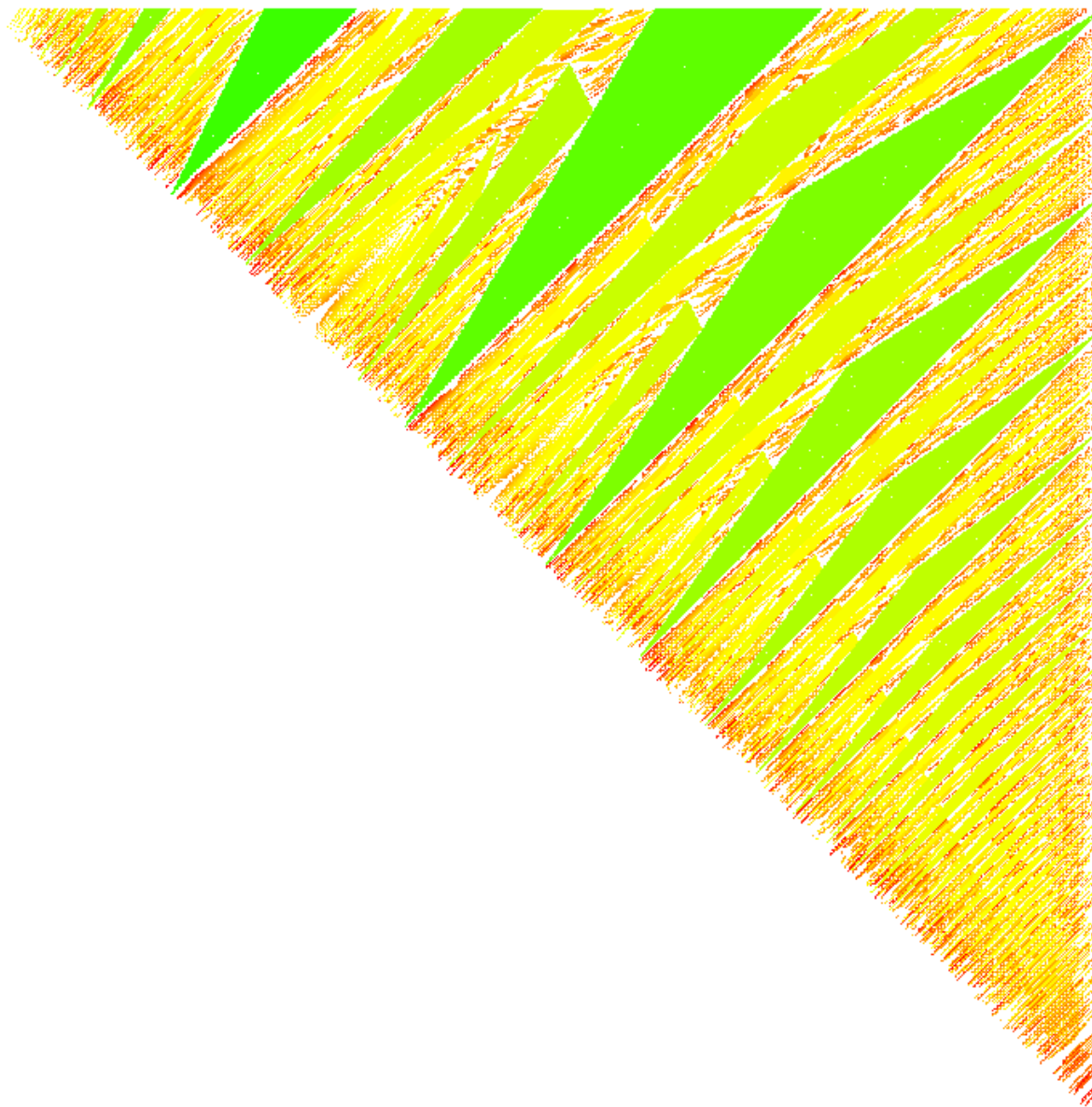


Figure 30: Detail of $\mathcal{S}(\mathcal{P}_0)$ in $[.4, .5] \times [.5, .6]$